Photosynth Res
DOI 10.1007/s11120-008-9351-9

REGULAR PAPER

D1-arginine257 mutants (R257E, K, and Q) of *Chlamydomonas reinhardtii* have a lowered Q_B redox potential: analysis of thermoluminescence and fluorescence measurements

Stuart Rose · Jun Minagawa · Manfredo Seufferheld · Sean Padden · Bengt Svensson · Derrick R. J. Kolling · Antony R. Crofts · Govindjee

Received: 25 June 2008 / Accepted: 6 August 2008

Abstract Arginine257 (R257), in the de-helix that caps the Q_B site of the D1 protein, has been shown by mutational studies to play a key role in the sensitivity of Photosystem II (PS II) to bicarbonate-reversible binding of the formate anion. In this article, the role of this residue has been further investigated through D1 mutations (R257E, R257Q, and R257K) in *Chlamydomonas reinhardtii*. We have investigated the activity of the Q_B site by studying differences from wild type on the steady-state turnover of PS II, as assayed through chlorophyll (Chl) *a* fluorescence yield decay after flash excitation. The effects of *p*-benzoquinone (BQ, which oxidizes reduced Q_B, Q_B^-) and 3-(3,4-dichlorophenyl)-1,1-dimethylurea (DCMU, which blocks electron flow from Q_A^- to Q_B) were measured. The equilibrium constants of the two-electron gate were obtained through thermoluminescence measurements. The thermoluminescence properties were changed in the mutants, especially when observed after pretreatment with 100 μM BQ. A theoretical analysis of the thermoluminescence data, based mainly on the recombination pathways model of Rappaport et al. (2005), led to the conclusion that the free-energy difference for the recombination of Q_B^- with S_2 was reduced by 20–40 mV in the three mutants (D1-R257K, D1-R257Q, and D1-R257E); this was interpreted to be due to a lowering of the redox potential of Q_B/Q_B^-. Further, since the recombination of Q_A^- with S_2 was unaffected, we suggest that no significant change in redox potential of Q_A/Q_A^- occurred in these three mutants. The maximum variable Chl *a* fluorescence yield is lowered in the mutants, in the order R257K > R257Q > R257E,

Jun Minagawa and Manfredo Seufferheld had equal credit in this work.

S. Rose · A. R. Crofts · Govindjee
Department of Biochemistry and Center for Biophysics and Computational Biology, University of Illinois at Urbana-Champaign, Urbana, IL 61801, USA

Present Address:
J. Minagawa
Institute of Low Temperature Science, Hokkaido University, Sapporo 060-0819, Japan

Present Address:
M. Seufferheld
Department of Natural Resources and Environmental Sciences (NRES), University of Illinois at Urbana-Champaign, 311 Edgar R. Madigan Lab (ERML), 1201 W. Gregory Drive, Urbana, IL 61801, USA

S. Padden
Physiological and Molecular Plant Biology Program, University of Illinois at Urbana-Champaign, 286 Morrill Hall, 505 S. Goodwin Ave., Urbana, IL 61801, USA

Present Address:
B. Svensson
Department of Biochemistry, Molecular Biology and Biophysics, University of Minnesota, 6-155 Jackson Hall, 321 Church St. SE, Minneapolis, MN 55455, USA

D. R. J. Kolling
Department of Chemistry, Princeton University, 17 Hoyt Laboratory, Washington Road, Princeton, NJ 08544, USA

Govindjee (✉)
Department of Plant Biology, University of Illinois at Urbana-Champaign, 265 Morrill Hall, 505 S. Goodwin Ave., Urbana, IL 61801, USA
e-mail: gov@illinois.edu; gov@uiuc.edu

compared to wild type. Our analysis of the binary oscillations in Chl *a* fluorescence following pretreatment of cells with BQ showed that turnover of the Q_B site was relatively unaffected in the three mutants. The mutant D1-R257E had the lowest growth rate and steady-state activity and showed the weakest binary oscillations. We conclude that the size and the charge of the amino acid at the position D1-257 play a role in PS II function by modulating the effective redox potential of the Q_B/Q_B^- pair. We discuss an indirect mechanism mediated through electrostatic and/or surface charge effects and the possibility of more pleiotropic effects arising from decreased stability of the D1/D2 and D1/CP47 interfaces.

Keywords D1-R257 mutants · Bicarbonate in Photosystem II · Thermoluminescence · Theory of thermoluminescence · Chlorophyll a fluorescence yield decay · Electron acceptor side of Photosystem II · Redox potentials of Q_A^-/Q_A and Q_B^-/Q_B · *Chlamydomonas reinhardtii* · Two-electron gate in Photosystem II · Benzoquinone

Abbreviations

BQ	*p*-Benzoquinone
C. reinhardtii	*Chlamydomonas reinhardtii*
Chl	Chlorophyll
18-Crown-6	Dicyclohexano-hexaoxacyclooctadecane
DCMU	3-(3,4-Dichlorophenyl)-1,1-dimethylurea
DMBQ	2,5-Dimethyl-*p*-benzoquinone
HS	High salt culture medium
ms	Millisecond(s)
PS II	Photosystem II
Ph	Pheophytin
Q_A	Primary plastoquinone electron acceptor of Photosystem II
Q_B	Secondary plastoquinone electron acceptor of Photosystem II
TAP	Tris–acetate–phosphate culture medium

Introduction

Photosystem II (PS II) turnover involves both a donor-side reaction mediated by the oxygen evolving complex, tyrosine Y_z, and chlorophylls (Chls) of the reaction center and an acceptor-side reaction involving pheophytin (Ph), a bound plastoquinone (Q_A), and an exchangeable plastoquinone (Q_B) (see reviews in Wydrzynski and Satoh 2005; Vassiliev and Bruce 2008). An electron leaving a specific Chl *a* molecule in the reaction center is transferred via the Ph to Q_A and subsequently to the exchangeable plastoquinone Q_B at the Q_B pocket. Electron transfer from Q_A^- to Q_B produces a semiquinone anion which is stabilized at the site and acts as acceptor in a second electron transfer that reduces the semiquinone to quinol, which then diffuses out of the Q_B pocket into the quinol pool. This sequence of two–one-electron transfer events and accompanying protonation reactions culminating in complete reduction of one quinone is known as the two-electron gate (Bouges-Bocquet 1973; Velthuys and Amesz 1974; Bowes and Crofts 1981; Robinson and Crofts 1983; Velthuys 1981; Wraight 1981). Bicarbonate (or carbonate) has been shown to have a unique effect on PS II reactions; it is involved in the functioning of the two-electron gate on the acceptor side (Govindjee et al. 1976; Eaton-Rye and Govindjee 1988a, b; reviews by Blubaugh and Govindjee 1988; van Rensen et al. 1999; van Rensen 2005). Further, bicarbonate (or carbonate) has been modeled in the recent PS II structures as a ligand to the Fe of the Q_AQ_B complex (Ferreira et al. 2004; Loll et al. 2005).

Since mutation of Arg257 (R257) of the D1 protein has previously been shown to modify bicarbonate-reversible formate binding, and to perturb electron transfer from Q_A^- to Q_B (Xiong et al. 1996), additional mutants were constructed to further investigate the role of this residue on equilibria in the two-electron gate. Structural models based on the bacterial reaction center template had indicated that R257 on the D1 protein is located close to the proposed Q_B-binding niche (Crofts et al. 1987; Bowyer et al. 1990; Ruffle et al. 1992; Xiong et al. 1996), and this has now been confirmed in recent crystallographic structures (Fig. 1; see "Discussion" section) (Ferreira et al. 2004; Loll et al. 2005; review: Kern and Renger 2007). In the present study, three substitutions of the arginine (R) residue have been constructed: lysine (K), glutamate (E), and glutamine (Q). All substituted residues have a smaller volume than arginine. Assuming aqueous p*K* values and physiological pH, arginine and lysine would be positively charged, and lysine would have similar electrostatic properties; the glutamate would be negatively charged; and glutamine would be neutral but polar, and with a similar volume to glutamate. In this article, we discuss the effects of mutation on the equilibria of the two-electron gate in the context of electrostatic changes mediated through coulombic and/or surface charge effects, and the possibility that the bicarbonate effect on the R257 mutants, observed earlier (Xiong et al. 1998a), might have a common basis in these local changes in charge. We also note the possibility of more pleiotropic effects resulting from decreased stability of the Q_B site on modification to the interfaces between D1 and its neighboring subunits, D2 and CP47.

Xiong et al. (1996) reported that replacement of R257 in *Chlamydomonas reinhardtii* with glutamate, R257E, or methionine, R257 M, did not greatly modify kinetics but

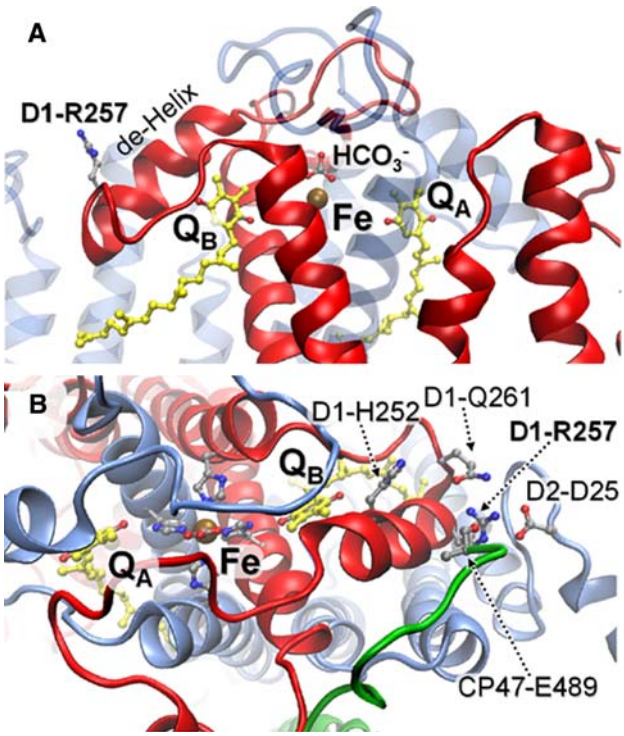

Fig. 1 Structure of the acceptor side of Photosystem II. **A** Location of the de-helix on the D1 protein. The D1 (red) and D2 (blue) proteins are shown in cartoon representation of the protein backbone. The loop of the D1 protein between transmembrane helices D and E of PS II is shown. D1-R257 mutated in this study is shown as ball-and-stick, located at the C-terminal end of the de-helix. The location of plastoquinones bound at the Q_A and Q_B sites are shown in yellow. The bicarbonate anion and the Fe atom to which it is ligated are shown as ball-and-stick and a van der Waals sphere, respectively. The orientation is parallel to the membrane plane. **B** Detailed view of the Q_B site and residues near D1-R257. Protein side chains are shown as ball-and-stick attached to a cartoon representation of the protein backbone. The D1 is red, D2 is blue, and CP47 is green. Q_A (yellow), the Fe atom and its ligands (the bicarbonate ion, and four histidines) are shown to the left of the image. Q_B is bound below the de-helix shown in the center of the image. To the right are D1-R257 and the nearby residues D1-Q261, D2-D25, and CP47-E489. The orientation is perpendicular to the membrane plane. Both **A** and **B** were created using VMD (Humphrey et al. 1996) from coordinates from PDB file 2AXT (Loll et al. 2005)

yielded a reduced sensitivity to the inhibition by formate treatment associated with a displacement of bicarbonate (Xiong et al. 1998a, b). Vernotte et al. (1995) had also noticed differential effects of bicarbonate-reversible formate effects on single and double mutants of D1 in *Synechocystis* sp. PCC 6714. In this study, we have introduced two additional substitution mutations, R257Q and R257K, in *C. reinhardtii* and examined the effects of these and the R257E mutation on the kinetics and equilibria of the two-electron gate, using Chl fluorescence. (For a more complete discussion of Chl fluorescence, see Papageorgiou and Govindjee 2004.) We examined the mutational effects on photoautotrophic growth, steady-state oxygen evolution, and Chl *a* fluorescence decay after a single flash of light. Cells of *C. reinhardtii* bearing these mutations were all photosynthetically competent but exhibited differences in the electron transfer from Q_A^- to Q_B that were also reflected in the growth rate and parameters used to describe the two-electron gate. The steady-state electron transfer in all mutants was slowed compared to wild type. The binary oscillation of Chl fluorescence of all the strains was altered, with the most dramatic change in the R257E strain. Interestingly, the R257E strain also shows a phenotypic response to a *p*-benzoquinone (BQ) titration—BQ is used to oxidize the plastoquinone pool affecting the electron transfer from Q_A^- to Q_B.

Thermoluminescence, originating in the recombination of the S_2 state of the donor side (Kok et al. 1970; see reviews in Wydrzynski and Satoh 2005) with the reduced state of the acceptor side of PS II, is reflected by the Q-band and the B-band (Rutherford et al. 1982; Sane and Rutherford 1986; Vass and Govindjee 1996) in the thermoluminescence curves. In the present work, we have used these measurements to explore the changes in energy of the charge-separated state (Inoue 1996; Vass 2003; Ducruet et al. 2007). On warming the sample that was preilluminated and then frozen, at a constant rate, thermal energy increases the probability of populating the excited state, and thermoluminescence occurs at a temperature reflecting the energy level of the charge-separated state (Vass and Govindjee 1996; Vass 2003). The spectrum of thermoluminescence is the same as that of fluorescence, indicating that the excited state populated on de-trapping is the same excited singlet state, P*, populated in the forward photochemistry (Inoue 1996). The general topological and thermodynamic framework for consideration of energy storage in PS II was established in the context of delayed fluorescence and the chemiosmotic hypothesis (Crofts et al. 1971). The different thermodynamic properties contributing to the driving force are the electrochemical contribution from ΔE_m of the redox participants; the chemical proton gradient, ΔpH; and the electrical field gradient, whose main contributor is the transmembrane potential difference, $\Delta\Psi$. In our experiments, the latter two components, representing the proton gradient, were largely dissipated by inclusion of dicyclohexano-hexaoxacyclooctadecane (18-Crown-6), which collapses the gradient (Lavergne 1984). We show that under these conditions the main contributions come from changes in ΔE_m and reflect changes on the acceptor side of PS II, localized in the reaction volume of the Q_B site.

In this study, thermoluminescence was measured on the D1-R257 mutants and the wild type cells. A major observation was that the B-band of thermoluminescence (due to $S_2Q_B^-$ recombination), from the mutants, was shifted to lower temperatures. The theoretical analysis of

thermoluminescence is usually based on a simple treatment of reaction kinetics developed by Randall and Wilkins (1945). In the context of thermoluminescence, the trapping and de-trapping pathways in a system are assumed to be the same. De Vault et al. (1983) and De Vault and Govindjee (1990) modified this scheme by considering that the recombination process in PS II involves an equilibrium between the various charge-separated states. Generally, this analysis provided conclusions that were limited to the change in the depth of the trap or the change in the free energy, appropriate for the analysis of the peak temperatures of the thermoluminescence bands. A more realistic goal of the theoretical analysis is to extract energy parameters that define specific steps in a physically relevant kinetic model of charge recombination in PS II. In this article, we have applied Rappaport et al. (2005) model (also see Cuni et al. 2004) and extended it with the equilibrium approach of De Vault et al. (1983) and De Vault and Govindjee (1990). The results of our extension of this theoretical analysis of thermoluminescence data allowed us to determine values of K'_{app}, the equilibrium constant between Q_A and Q_B; previously, values of K'_{app} had been obtained from Chl *a* fluorescence decay and binary oscillations in fluorescence in *C. reinhardtii* cells (Crofts et al. 1993), based on a recombination model proposed by Robinson and Crofts (1983) and Taoka and Crofts (1987). Rappaport et al. (2005) had performed both fluorescence and thermoluminescence measurements on *C. reinhardtii* cells having mutations that changed the midpoint potential of the primary acceptor of PS II, Ph, to characterize energetic parameters in the recombination of electrons from Q_A^- with S_2 in 3-(3,4-dichlorophenyl)-1,1-dimethylurea (DCMU)-treated samples. The change of the midpoint potential of a recombination intermediate did not affect the depth of the trap but did change thermoluminescence. Rappaport et al. (2005) had taken into account the multiple pathways for charge separation and recombination, but only one pathway produced light during thermoluminescence measurements. Following this approach, we have measured and analyzed both fluorescence decay and thermoluminescence after one or two flashes. On this basis, we conclude that the redox potential of Q_B/Q_B^- is lowered in the D1-R257E, Q, and K mutants of *C. reinhardtii* cells.

Materials and methods

Site-directed mutagenesis

Mutations were generated in the plasmid pBA157, previously developed to facilitate site-directed mutagenesis of the *psbA* gene, by mutagenic primer-directed PCR (Minagawa and Crofts 1994). After confirmation of the mutational lesion by sequencing of the entire region subjected to PCR amplification, the mutagenized plasmids were shot into a *psbA* deletion mutant of *C. reinhardtii*. In addition to mutations constructed earlier (D1-R257E and D1-R257M, Xiong et al. 1998a), the codon for arginine257 (CGA) was altered to lysine (AAG) and glutamine (CAA) using mutagenic primers:

5′-TTGGAAGATTAGCTTACCAAAGTAACC-3′ (antisense); 5′-TTGGAAGATTAGTTGACCAAAGTAACC-3′ (antisense).

To obtain D1-R257K and D1-R257Q mutants, site-directed mutagenesis was performed by the Megaprimer method (Sarkar and Sommer 1990) using P3 forward and R6 reverse primers and native *Pfu* polymerase from Stratagene (La Jolla, CA). The resultant DNA fragments were tailored by restriction enzymes, *Pst*I and *Bgl*II, and replaced with the counterparts in the plasmid pBA157. Transformation of a *psbA* deletion mutant, ac-u-ε, by the mutated plasmids was performed, as described previously (Minagawa and Crofts 1994). The mutations on the plasmid DNA and on the chloroplast genome of the transformants were confirmed for both strands by automated DNA sequencing performed by Genetic Analyzer ABI PRISM 310 (PE Biosystems, Foster City, CA). Further technical details were as described previously (Xiong et al. 1998a).

Growth of cells

The wild type (control) and mutant strains were maintained in TAP (Tris–acetate–phosphate culture medium) agar plates with spectinomycin. Ampicillin was added to the plates to prevent bacterial contamination. These cells were then grown at 25°C under low white light ($\sim$3–7 μE m^2 s^{-1}) in liquid TAP medium (20 mM Tris; 17.4 mM acetate; 7 mM NH_4Cl, 0.4 mM $MgSO_4$, 0.3 mM $CaCl_2$, 1 mM phosphate buffer, 1 ml/l Hutner's trace metal solution; the pH was adjusted to 7 with dilute acetic acid; Gorman and Levine 1965). Cells for measurements of oxygen evolution, fluorescence kinetics, and thermoluminescence were harvested when they reached the early logarithmic phase ($\sim 2 \times 10^6$ cells/ml).

To measure growth rates under photoautotrophic conditions, cells were washed once and used to inoculate a high salt (HS) liquid minimal medium (9 mM NH_4Cl, 0.08 mM $MgCl_2$, 9 mM NH_4Cl, 0.06 mM $CaCl_2$, 13.5 mM phosphate buffer; Sueoka 1960). Cells used for measuring photosynthetic growth rates were grown at 25°C under 100 μE m^{-2} s^{-1} illumination, and the cell suspension was bubbled with air containing 3% CO_2 (v/v).

Cell density was determined by optical density (OD) measurements at 750 nm in a cuvette with a 1-cm light path using a MPS-2000 spectrophotometer (Shimadzu Co.,

Kyoto, Japan). For the accurate measurement of OD_{750}, the original cultures were diluted before the measurement to avoid OD values over 0.5.

Determination of chlorophyll concentration

For Chl concentration determinations, we used either the equations of Porra et al. (1989) after extraction of whole cells with 80% acetone or of Harris (1988) after extraction with 95% ethanol.

Assay of oxygen evolution

Steady-state oxygen evolution activity of the cells was measured in TAP medium with a Clark-type oxygen electrode in the presence of 0.5 mM 2,5-dimethyl-*p*-benzoquinone (DMBQ) and 2 mM $K_3Fe(CN)_6$ at 25°C under illumination at 3,000 μE m^{-2} s^{-1}. Each strain was assayed in at least two separate cultures, with an average of three measurements for a single culture.

Chlorophyll *a* fluorescence yield decay: flash-induced kinetics and binary oscillations

To test if the D1 mutants (R257E, Q, and K) were altered on the electron acceptor side of PS II, fluorescence kinetic measurements were performed with a laboratory-built fluorimeter (Kramer et al. 1987; Kramer and Crofts 1990; T. Miller and A. R. Crofts, personal communication, 2000). Brief (7 μs) actinic flashes (greater than 90% saturating) were provided by a Xenon discharge flash lamp (1,500 V, 3 μF). The Xenon bulb was made by EG&G and doped with hydrogen for faster quench, to allow for more rapid succession of flashes. Two optical filters, a blue glass filter (Schott, BG7) and a heat filter (Melles Griot, KG3), were placed between the sample and the discharge flash lamp to select blue exciting light and block light corresponding to the measuring wavelengths of light.

A rapid series of low intensity red light pulses from an array of light emitting diodes (LEDs) was given to the sample to resolve kinetics of Chl fluorescence yield changes on a sub-ms time scale after each actinic flash. Each measuring pulse typically had an actinic effect of less than 1% of saturation; it was provided by eight 5-mm high-performance Al–Ga–As red LEDs (Agilent, HLMP-8103), which had a wavelength maximum at 644 nm. The actinic light was filtered with an interference filter with a peak at 635 nm and a half bandwidth of 35 nm (Omega, 635-DF70). Variable Chl *a* fluorescence was detected by a photodiode screened by a red cut-off filter (Corning, CS2-64; 50% transmission at 695 nm) and recorded as a function of time, *t*, after the actinic flash, as the normalized yield of variable fluorescence ($F_v = (F_t - F_0)/F_0$) measured from the fluorescence at time *t* (F_t) and the fluorescence immediately before the actinic flash (F_0).

Chlorophyll *a* fluorescence yield decay was measured after each of two saturating actinic flashes 1 s apart. Each flash was followed by a series of measuring pulses at time intervals of 0.065, 0.195, 0.325, 0.700, 1.25, 2.50, 5.0, and 9.95 ms after the flash at zero time. Samples for measurement were cell cultures that were 6–7 days old. Samples from the culture medium were treated with 100 μM BQ for 10 min in the dark. The cells were then collected by centrifugation, resuspended in 800 μl of TAP medium, and diluted to a final Chl concentration of 7 μg/ml, in a volume of 2.4 ml. Because of the variability of effect of BQ on fluorescence yield, the values for τ (the characteristic time, or the lifetime, given by 1/rate constant) were derived directly from the data, without correction for either the maximal fluorescence yield in the presence of DCMU or the redistribution of excitation between centers due to connectedness of the antenna. As a consequence, the reported rates are somewhat faster than those previously reported (Crofts et al. 1993).

For measuring DCMU-treated cells, samples were prepared as for the preceding experiment, and then DCMU was added to a final concentration of 10 μM. The cells were further dark adapted for 10 min and then subjected to a single actinic flash, followed by a train of measuring pulses with time intervals up to 10 s. The fluorescence yield data were recorded and exported for analysis using *Origin 8* (Origin Lab, Northampton, MA). Each curve was an average of three independent measurements.

In order to measure the effect of varying BQ concentration during pretreatment, cultures were prepared in the same manner as for the preceding two-flash experiment except that samples of cells were collected after pretreatments with three different concentrations of BQ (10, 25, and 100 μM). An average of three measurements from three samples was used for each BQ concentration. A decrease in F_0 values for the samples with 100 μM BQ was observed, likely due to fluorescence quenching by the added BQ (Amesz and Fork 1967).

Binary oscillations in Chl fluorescence decay kinetics, due to the different electron transfer rates from Q_A^- to Q_B, or Q_B^- (Velthuys and Amesz 1974; Bowes and Crofts 1980; Eaton-Rye and Govindjee 1988a, b), were measured by applying a series of actinic flashes spaced at 1 s intervals, and recording the kinetics of fluorescence yield decay ($F_v = (F_t - F_0)/F_0$) after each flash. Binary oscillations were maximal when measured at 150–250 μs after the actinic flashes; the values at 195 μs are shown here. Cells were dark adapted for 10 min and treated in dark with 10, 25, or 100 μM BQ. Cells were pelleted by centrifugation and then resuspended in fresh TAP medium. The concentration was adjusted to 7 μg of Chl *a*/ml.

Thermoluminescence measurements and analysis

Thermoluminescence was measured with a laboratory-built instrument (Kramer et al. 1994). Cell suspensions containing ~5 μg Chl *a*/ml in the growth medium were first illuminated with weak continuous white light for 20 s at 20 ± 2°C and then centrifuged. The cells were resuspended in 1 ml of medium containing 10 mM NaCl, 5 mM $MgCl_2$, 25 mM MES, pH 6.5, and 1 μM 18-Crown-6 (Sigma, Product No: D2637); the latter was used as an ionophore (Lavergne 1984) to eliminate variability due to contributions to the stored free energy from the proton gradient. The cell suspensions were incubated in the dark for 5 min at 20 ± 2°C. To measure thermoluminescence originating from $S_2Q_A^-$ charge recombination (Q-band, Rutherford et al. 1982; Vass and Govindjee 1996), the cells were incubated for 5 min at room temperature with 10 μM DCMU, which displaces Q_B (Velthuys 1981), and thus blocks reduction of Q_B by reduced Q_A. To record thermoluminescence due to charge recombination from Q_B^- (B-band), the DCMU treatment was omitted. Where indicated, the samples were pretreated with different concentrations of BQ. The samples were then washed and resuspended in 1 ml of the above medium, but lacking DCMU and the 18-Crown-6, to remove BQ that could interfere with the acceptor-side reactions. The cells were then concentrated to 1 mg Chl *a*/ml by centrifugation. The cell suspension (10 μl) was used in the sample chamber of the instrument. After dark adaptation for another 5 min at 20°C, the sample was cooled to −10°C and a saturating Xenon flash was given. After the saturating flash, the samples were then rapidly cooled to −50°C. Thermoluminescence was recorded as the samples were heated at a rate of 0.7°C/s, from −50 up to 50–60°C.

Theoretical analysis

The equations used included parameters for three pathways for recombination of the photochemical products. The three competing recombination pathways are involved in the recombination of the electron on Q_A^- with P^+ (this P does not distinguish between $P_{D1}{}^+$ and Acc-Chl *a* (D1); Rappaport et al. 2002). Two non-radiative pathways were proposed: the first (direct) and involving recombination from Q_A^- to P^+ to form Q_A and P and the second (indirect) via the primary acceptor, Ph. Both of these pathways result in thermal de-excitation. The last pathway results in the formation of the excited singlet state P* followed by radiative decay, as shown below:

$$[(\text{Photochemical products}) \leftrightarrow P^+Ph^- \leftrightarrow P^*Ph \xrightarrow{h\nu} PPh].$$

The scheme proposed by Rappaport et al. (2005) uses three different rate constants corresponding to each of the three pathways, as mentioned above. The overall rate constant for recombination is the sum of the separate rate constants, each of which can be represented in Arrhenius form:

$$\begin{aligned} k_{\text{tot}}(T) &= k_{\text{r}}(T) + k_{\text{d}}(T) + k_{\text{ex}}(T) \\ &= s_{\text{r}} e^{\frac{-\Delta H_{\text{r}}}{k_{\text{B}}T}} + s_{\text{d}} e^{\frac{-\Delta H_{\text{d}}}{k_{\text{B}}T}} + s_{\text{ex}} e^{\frac{-\Delta H_{\text{ex}}}{k_{\text{B}}T}} \end{aligned} \quad (1)$$

where the subscripts r, d, and ex correspond to the indirect, direct, and excitonic recombination routes, respectively; ΔH values are enthalpies of activation; and s values are Randall–Wilkins pre-exponential terms given by $s = \kappa \exp\{\Delta S/k_B\}$, where k_B is the Boltzmann constant; ΔS is the entropy of activation; and κ represents an intrinsic rate constant containing terms determined by the path, and the vibrational frequency, $k_BT/h = 10^{13}\ s^{-1}$ (Rappaport et al. 2005), most simply approached through the Moser–Dutton treatment (Moser et al. 1997, 2006). In the thermoluminescence scheme, the luminescence intensity $L(T)$, in the presence of DCMU (i.e., when no sharing of electrons on the acceptor side occurs), can be derived from the recombination rate, $dn(T)/dt$, as below. The recombination rate at temperature T is

$$\frac{dn(T)}{dt} = -k_{\text{tot}}(T)n(T) \quad (2)$$

which, at a fixed warming rate, $B = dT/dt$, is equal to

$$\frac{dn(T)}{dT} = \frac{-k_{\text{tot}}(T)}{B} n(T) \quad (3)$$

The luminescence intensity is given by the fraction of decay determined via k_{ex}:

$$L(T) = \phi k_{\text{ex}}(T)n(T) \quad (4)$$

where ϕ is the fluorescence yield, accounting for the partitioning of excitation decay to radiative and non-radiative pathways (Lavorel 1968; Rappaport et al. 2005).

The equation for $L(T)$, Eq. 4, when solved by substituting $n(T)$ from the integrated form of Eq. 3 results in the following expression for the peak temperature, T_m, at the maximum, where $dL(T)/dT = 0$:

$$\frac{\Delta H_{\text{ex}}}{k_{\text{B}}T_{\text{m}}^2} = \frac{1}{B} k_{\text{tot}}(T_{\text{m}}) \quad (5)$$

Parameters for Eq. 5 have already been investigated for *C. reinhardtii* (Cuni et al. 2004; Rappaport et al. 2005).

With the Rappaport et al. (2005) model as a starting point, we now introduce the equilibria of the acceptor side. Recombination depends on the fractional occupancy of the substrate Q_A^-, determined by the equilibration in the two-electron gate (Crofts et al. 1971; Rutherford et al. 1982; De Vault et al. 1983; De Vault and Govindjee 1990; Robinson and Crofts 1983). The fraction of carriers, $\chi(T)$, available

for recombination, is defined by the equilibrium constant, K, and is equal to:

$$\chi(T) = \frac{K(T)}{1 + K(T)} = \frac{[Q_A^-]}{n(T)} \tag{6}$$

where $n(T) = [Q_A^- Q_B] + [Q_A Q_B^-]$, the total number of electrons available for recombination on the acceptor side. K here is the overall equilibrium constant determining the fraction of centers in which the electron is on Q_A, equivalent to K_{app} (if partitioning into K_E, pK_3 and K_O is known) or K'_{app} (if partitioning is not known, as in this study).

In the absence of a proton gradient, the equilibrium constant $K(T)$ between $Q_A^- Q_B$ and $Q_A Q_B^-$ is determined by the free-energy difference, $\Delta G_{ab} = -zF\Delta E_{Q_B - Q_A}$ through $K = \exp(-\Delta G_{ab}/k_B T)$, equivalent to K'_{app} here.

Substituting from Eq. 6, the recombination rate from Eq. 3 becomes

$$\frac{dn(T)}{dT} = \frac{-1}{B} k_{tot}(T)\chi(T)n(T) \tag{7}$$

And the thermoluminescence intensity is then given by

$$L(T) = \phi k_{ex}(T)\chi(T)n(T) \tag{8}$$

The Rappaport et al. model (2005) was used to simulate thermoluminescence data to allow comparison with the measured data. We developed two treatments for the data analysis. The first was a non-linear regression, which searched for a least squares fit to a model using the Levenberg–Marquardt method. The second was a peak analysis equation which was developed from the derivative of the solved equations and solved iteratively at the corresponding peak temperature. The differential equations used in Rappaport et al. (2002) to describe thermoluminescence were set up and solved in the *Mathematica* (Wolfram Research Inc., Champaign, IL). The resulting solution was an interpolated function because an exact analytical solution does not exist. The equations were used to generate values for the equilibrium constant determining fractional occupancy of the acceptor side states from the glow curves. For analysis of glow curves in the absence of DCMU, Eq. 7 was rearranged, and integrated, then solved for $n(T)$, the total number of electrons on the acceptor side, using Eq. 6 to give, on substitution into $L(T)$ in Eq. 8:

$$L(T) = \phi k_{ex}(T)\chi(T) \exp\left\{\frac{-1}{B}\int_{T_0}^{T} k_{tot}(x)\chi(x)dx\right\} \tag{9}$$

Here, B is the rate of heating, and x is included as a variable of integration across the temperature range. For purposes of peak analysis, the thermoluminescence is unchanging over the peak, so

$$\frac{dL(T_m)}{dT} = 0 \tag{10}$$

After differentiating Eq. 9, substituting in T_m, and setting the result to 0, the following equation must hold as a solution of Eq. 10:

$$e^{\frac{-\Delta G_{ab}(T_m)}{k_B T_m}}(\Delta H_{ex} - \Delta G_{ab}(T_m)) = \frac{k_B}{B} T_m^2 k_{tot}(T_m) - \Delta H_{ex} \tag{11}$$

where $\Delta G_{ab}(T_m)$ and $k_{tot}(T_m)$ are the values of ΔG_{ab} (defined as in the discussion of Eq. 6) and k_{tot}, respectively, at the peak temperatures, and k_B is the Boltzmann constant. This equation is an expanded version of Eq. 5 that includes terms for the extra contribution from the acceptor complex to the occupancy of back-reaction substrate.

For the thermoluminescence curves in the presence of DCMU, we used Eq. 5, and values for s_r, s_d, ΔH_d from Rappaport et al. (2005), and calculated values of ΔH_{ex} which satisfied the equation for the measured peak temperature T_m of the Q-band. Using the additional constraint that the radiative yield was 1–3%, values for ΔH_r of 637 mV and ΔH_{ex} of 685 mV were found.

For the glow curves in the absence of DCMU, Eq. 11 was used. The temperature dependency of ΔG_{ab} and k_{tot} was included through $\Delta G_{ab}(T)$ and $k_{tot}(T)$, assuming that the entropy contribution to ΔG_{ab} was negligible. Using this equation, the values of s_r, s_d, ΔH_d from Rappaport et al. (2005), and the values ΔH_{ex} (as 685 mV) and ΔH_r (as 637 mV) calculated for the Q-band, we deduced the ΔG_{ab} and K'_{app} values at T_m as shown later in Table 5 (see "Results"). These values compare well with the values obtained by Crofts et al. (1993) directly from fluorescence decay measurements.

Results

Growth rate

Figure 2 shows the time-course of photoautotrophic growth of the R257 mutants and a wild type control in a minimal medium under 100 μE m^{-2} s^{-1} illumination. The relative growth of the mutant strains and the pBA157 control, as measured by OD_{750}, after 5 days of growth, is shown in Table 1. In the early logarithmic phase ($OD_{750} < 0.2$), R257Q and R257K mutants had a doubling time of 7–8 h, which was only slightly longer than that of the wild type control, pBA157. The R257E mutant showed a significantly slower growth rate where the doubling time was 9–10 h. In the later growth phases, differences were more prominent. The cell culture of the pBA157 control reached a density corresponding to an OD_{750} value of 2.2 after

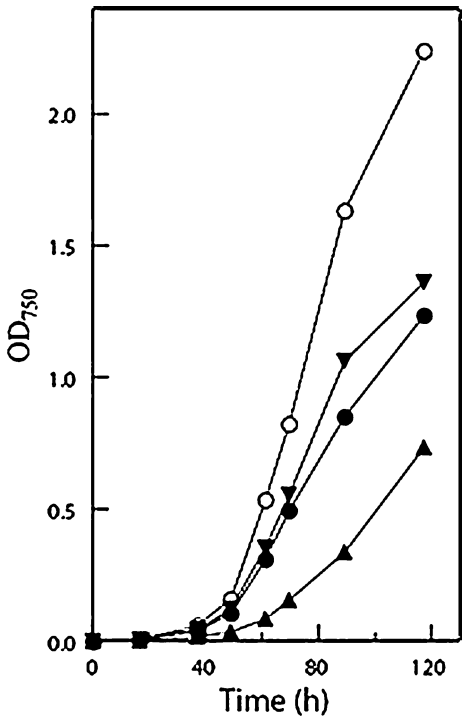

Fig. 2 Photoautotrophic growth. *C. reinhardtii* cells were grown in high salt minimal medium (Sueoka 1960) at 25°C, bubbled with 3% CO_2 (v/v), and illuminated with 100 μE m^{-2} s^{-1} white light. The growth curve was determined by measuring the optical density (OD) of the cell suspension at 750 nm. Wild type control, pBA157 (open circles); R257K (upside down triangles); R257Q (closed circles); R257E (triangles)

5 days. The R257Q and R257K mutants reached a final density (OD_{750}) of 1.3 and 1.4, respectively. The R257E mutant only reached an OD_{750} value of 0.7.

Oxygen evolution

Table 1 shows the measured steady-state oxygen evolution activity in the arginine mutants and the wild type control. The rate of oxygen evolution for wild type, pBA157, reported by Xiong et al. (1998a) was close to the value reported in Table 1; the mutants, R257K, R257Q, and R257E had, respectively, 82%, 71%, and 37% activity of the wild type control. This is comparable to the relative values in levels of culture density after 5 days of photoautotrophic growth. The lower level of culture density in the mutants, especially in R257E mutant, parallels their lower electron transfer activity (on a Chl basis) from water to the artificial electron acceptor at the Q_B site, DMBQ.

Chlorophyll *a* fluorescence decay after first and second actinic flashes with BQ pretreatment

Pretreatment with BQ was used to re-oxidize the electron acceptor pool of PS II, the plastoquinone pool, and the occupant of the Q_B site. BQ was removed by washing before the kinetic experiments were performed (see Crofts et al. 1993; also see "Discussion" section). Since pretreatment with 100 μM BQ, added to the cell suspension, showed significant effects on thermoluminescence bands (see later), we also measured Chl fluorescence yield decay under similar conditions. Figure 3 shows the Chl fluorescence decay curves for the wild type, pBA157 (panel A), for R257K (panel B), for R257Q (panel C), and for R257E (panel D) of *C. reinhardtii*. Squares are for fluorescence decay after first flash (black curve) and circles after a second flash (red curve), given 1 s after the first. Insets in each of the panels show the sub-ms data of the corresponding curves in that panel. These data show small, but reproducible, differences between the Chl *a* fluorescence decay after first and second flashes; the two-electron gate is functional, and there are quantitative differences between the different mutants. The R257Q mutant showed the largest difference in the decay after the first and the second flash. Table 2 shows the characteristic times, or lifetimes, τ, for these fluorescence decay curves; these times for the fast phase after the second flash are clearly longer than after the first flash except for R257E strain.

Chlorophyll *a* fluorescence decays after one flash in the presence of 3-(3,4-dichlorophenyl)-1,1-dimethylurea

The fluorescence decay of the wild type control strain (pBA157) and the three mutant strains (R257K, R257Q,

Table 1 Growth comparison and steady-state oxygen evolution activity for wild type and D1-R257 mutant strains. Oxygen evolution activity of the cells was measured in TAP medium in the presence of 0.5 mM 2,5-DMBQ and 2 mM $K_3Fe(CN)_6$ at 25°C under illumination at 3,000 μE m^{-2} s^{-1}

Strain	Autotrophic growth			O_2 evolution activity	
	OD_{750} (after 5 days)	Wild type (%)	Growth rate (doubling $time^{-1}$), wild type (%)	μM O_2/mg Chl/h	Wild type (%)
Wild type	2.2	100	100	186.1 ± 10.5	100
R257K	1.4	64	80–85	152.6 ± 7.9	82
R257Q	1.3	59	80–90	131.9 ± 8.8	71
R257E	0.7	38	50–60	69.9 ± 6.6	37

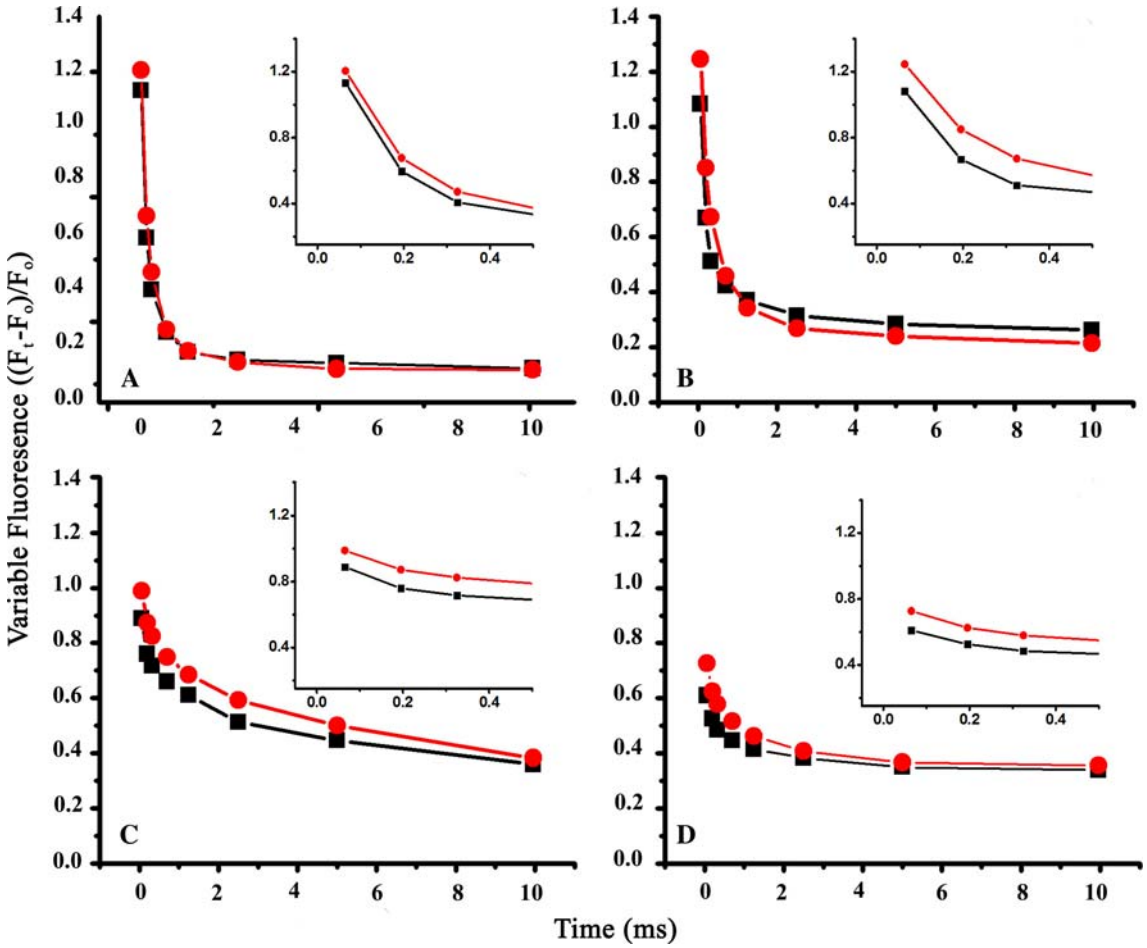

Fig. 3 Variable Chl *a* fluorescence decay curves, after flashes 1 or 2 (at 1 Hz). Samples from 6 to 7 days old *C. reinhardti* cultures were treated with 100 μM BQ for 10 min in the dark. Panel **A** is for pBA157, previously shown to act as wild type; panel **B** is for R257K; panel **C** for R257Q, and panel **D** for R257E. The first flash is designated by squares (black curve), the second flash by circles (red curve). Insets in each of the panels show the sub-ms data of the corresponding curves in that panel. The standard error was approximately the size of the symbols used. F_t is fluorescence at time t, and F_0 is the initial minimal fluorescence. [Chl], 7 μg/ml

Table 2 The characteristic lifetimes ($\tau = 1$/rate constant) of fluorescence yield decay curves after treatment with 100 μM benzoquinone followed by washing with Tris–acetate–phosphate buffer

Strain	First flash		Second flash	
	Fast phase (μs)	Slow phase (ms)	Fast phase (μs)	Slow phase (ms)
pBA157	110 ± 10	0.65 ± 0.16	131 ± 20	0.71 ± 0.16
R257K	118 ± 10	1.70 ± 0.27	151 ± 30	0.92 ± 0.19
R257Q	116 ± 40	3.31 ± 0.6	198 ± 40	4.58 ± 0.88
R257E	146 ± 10	2.05 ± 0.18	140 ± 20	1.54 ± 0.11

and R257E) when pretreated with 100 μM BQ and then with 10 μM DCMU are shown in Fig. 4 on a log time scale. Experiments, presented here, included measurements up to 10 s to include all the slow back reactions involved in the PS II reactions. The fluorescence yield levels of all the mutant strains start out at a lower value than the wild type; the R257E mutant had ~35% yield, whereas R257K and R257Q had ~80% yield of the wild type. Further, the F_0 value for R257E was 50% of wild type (pBA157) in the presence of DCMU (Xiong et al. 1998a). No significant change in the kinetics of fluorescence yield decay was immediately apparent.

BQ titration of the R257E mutant

Since BQ pretreatment played a significant part in this paper, we present here fluorescence data on the effect of three different BQ concentrations on a selected mutant

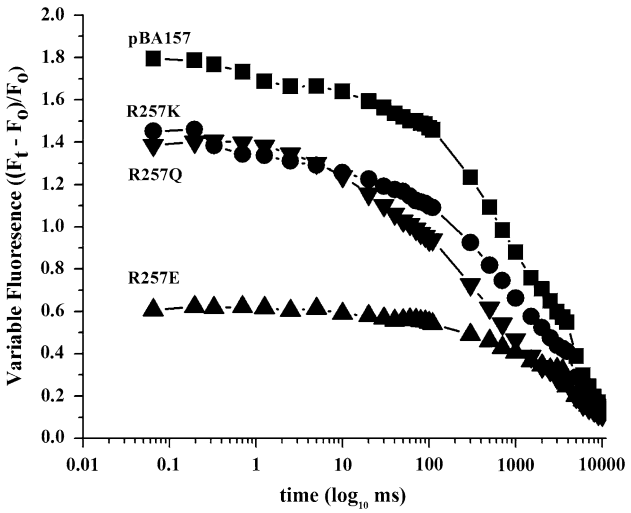

Fig. 4 Variable Chl *a* fluorescence decay curves in the presence of DCMU. Cells of three mutants (R257K, R257Q, and R257E) and the wild type (pBA157) *C. reinhardtii* were treated as in Fig. 3. DCMU was added to a final concentration of 10 μM. A single actinic flash was delivered after 10 min dark adaptation with the DCMU present. A train of measuring pulses was used up to 10 s. F_t is fluorescence at time t, and F_0 is the initial minimal fluorescence. [Chl], 7 μg/ml

(R257E), as an example. Figure 5 shows the decay of Chl *a* fluorescence yield for R257E cells at 10 μM BQ (panel B), 25 μM BQ (panel C), and 100 μM BQ (panel D) as well as in untreated samples (panel A). The graph in each panel shows results after flash 1 (squares; black curve) and flash 2 (circles; red curve). Table 3 shows the biphasic decay kinetic parameters for the R257E mutant cells. (The R257E mutant, which had the lowest fluorescence yield (Fig. 4), showed larger variations among different cultures.) In the first phase of fluorescence decay, the differences after flash 1 and after flash 2 were larger at higher BQ concentrations (Fig. 5). However, the calculated lifetime of the fast phase after flash 2 was shorter than after flash 1 (Table 3).

The Q_A^- oxidation rate (as inferred from Chl *a* fluorescence decay) appeared to be slower, as compared with the untreated sample, with even small amounts of BQ treatment (25 μM) (Fig. 5), but this reflects mainly the anomalous quenching by BQ. At 100 μM BQ, the Chl *a* fluorescence decay was virtually eliminated (Fig. 5, panel D); this reduction in the Chl fluorescence yield is consistent with the loss of thermoluminescence (see "Discussion" section).

In order to test the hypothesis that the BQ may be changing the structure of the Q_B pocket, a DCMU titration assay was performed comparing wild type to the R257E strain. There was no apparent change in the I_{50} ($\sim$500 nM) between the wild type and the R257E, which suggests that the Q_B pocket is not significantly perturbed by the mutation.

Chl *a* fluorescence oscillations as a function of number of actinic flashes

Figure 6 shows clearly the existence of a functional two-electron gate in the wild type (panel A) as well as in R257K (panel B), R257 Q (panel C), and R257E (panel D) mutants. These binary oscillations are most obvious when the samples were pretreated with 100 μM BQ (squares) and even with 50 μM BQ (circles) showing the usefulness of using BQ in our studies. Further, these binary oscillations are clearest in R257Q (panel C), followed by the wild type and R257K, with R257E having the least visible binary oscillations. These differences are related to the differences caused by the modification of the Q_B pocket by the mutations, and the further effects of BQ in interaction with the site, or with the antenna apparatus.

Thermoluminescence characteristics in the presence of DCMU

Thermoluminescence data for the control and the D1-Arg257 mutants illuminated with a single-turnover flash in the presence of 10 μM DCMU are shown in Fig. 7. Mean peak temperatures of the thermoluminescence curves are summarized in Table 4. Addition of DCMU, which blocks oxidation of Q_A^- by Q_B, induces a major thermoluminescence peak at around 10°C, known to originate from the $S_2Q_A^-$ recombination (Q-band) (Rutherford et al. 1982, 1984; De Vault et al. 1983; Vass and Govindjee 1996). All three mutants showed a Q-band in the 11–13.5°C range, which, within experimental reproducibility, is essentially the same as for the control cells. As mentioned earlier, the peak temperature of a thermoluminescence component is indicative of the driving force for reversal of the photochemical reaction arising from the stored work in a separated pair of charges, which reflects redox properties of both the recombination partners. These results suggest that the overall stability of $S_2Q_A^-$ charge pair was not affected by the mutations at D1-R257.

Thermoluminescence of untreated samples and samples pretreated with BQ

The thermoluminescence emission peak at 35–40°C (B-band) is known to result largely from the recombination of the $S_2Q_B^-$ and $S_3Q_B^-$ charge pairs (see e.g., Vass and Govindjee 1996). Figure 8 (panel A) shows the thermoluminescence curves for the wild type and the three R257 mutant strain cells that were not treated with BQ or the inhibitor DCMU. Figure 8 (panel B) shows thermoluminescence curves for 25 μM BQ-treated cells, whereas Fig. 8 (panel C) shows results for 100 μM BQ-treated cells. Mean peak temperature values for the

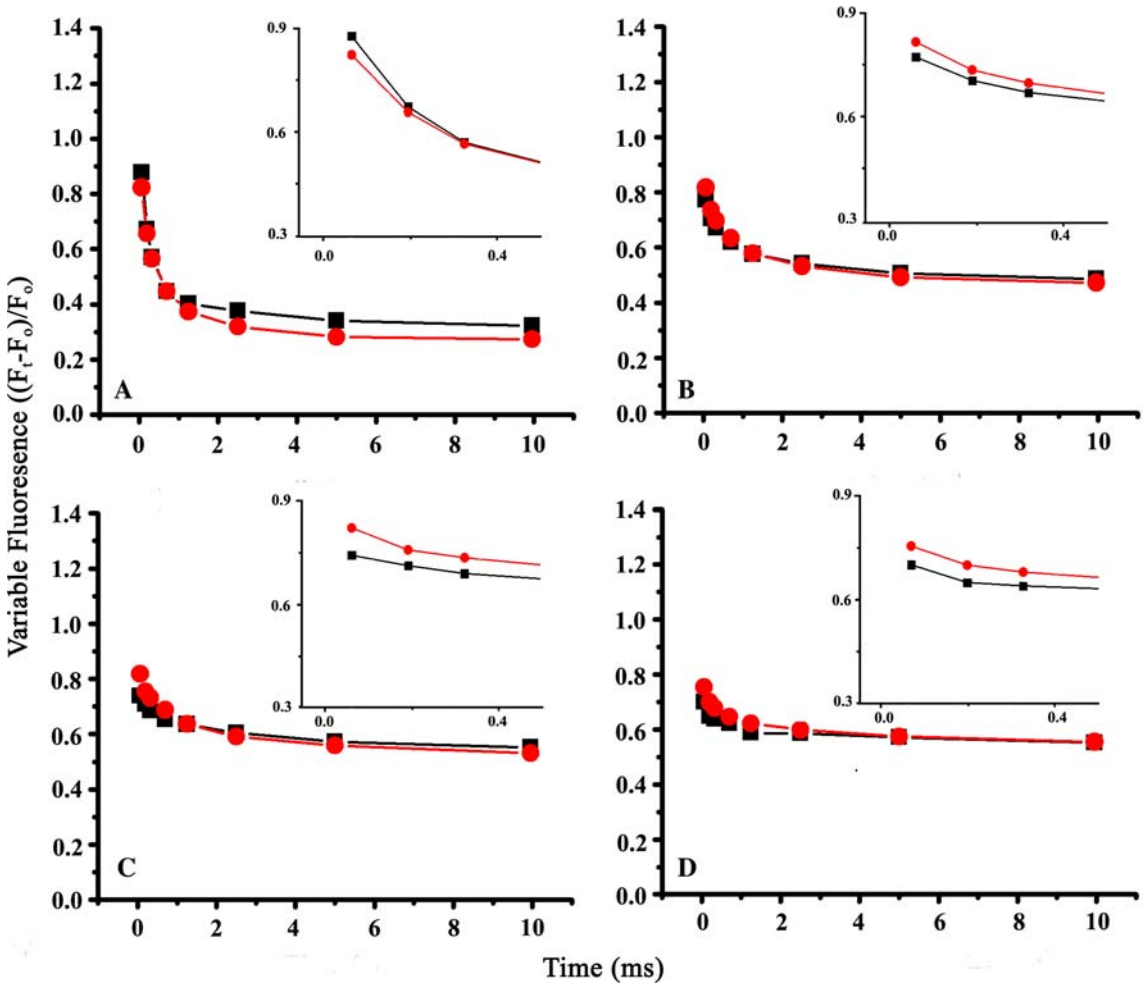

Fig. 5 Variable Chl *a* fluorescence decay curves in the R257E mutant of *C. reinhardtii* cells, pretreated with different BQ concentrations. Panel **A** is in the absence of BQ; panel **B** is with 10 μM BQ; panel **C** is with 25 μM BQ, and panel **D** is with 100 μM BQ. The first flash is designated by squares (black curve), the second flash by circles (red curve). Seven-day-old *C. reinhardtii* cultures of the R257E strain were used, dark adapted for 10 min. F_t is fluorescence at time t, and F_0 is the initial minimal fluorescence. [Chl], 7 μg/ml

Table 3 The characteristic lifetimes, τ (inverse of rate constant, k) of fluorescence yield decay curves for R257E at indicated concentrations of benzoquinone (BQ)

R257E BQ concentration (mM)	First flash		Second flash	
	Fast phase (μs)	Slow phase (ms)	Fast phase (μs)	Slow phase (ms)
0	217 ± 10	2.86 ± 0.58	207 ± 20	1.37 ± 0.18
10	243 ± 40	2.41 ± 0.47	213 ± 50	1.88 ± 0.32
25	248 ± 30	3.09 ± 0.29	130 ± 70	1.79 ± 0.36
100	193 ± 10	3.35 ± 1.99	137 ± 160	1.82 ± 0.49

These experiments were performed with whole cells from a different culture to those in Table 2

thermoluminescence data on varying the amount of BQ are shown in Table 4. Mean peak temperature is the average of the maximum or peak temperature for five different thermoluminescence data sets. Values for thermodynamic parameters calculated from these peaks are shown in Table 5 and discussed below.

As shown in Fig. 8 (panel A), with no pretreatment, there are two peaks in the thermoluminescence curve for wild type (pBA157) cells. The maximum of the higher temperature peak for the wild type curve in Fig. 8 (panel A) is about 40°C and corresponds to the mean peak temperature of ~42°C listed in Table 4. The lower

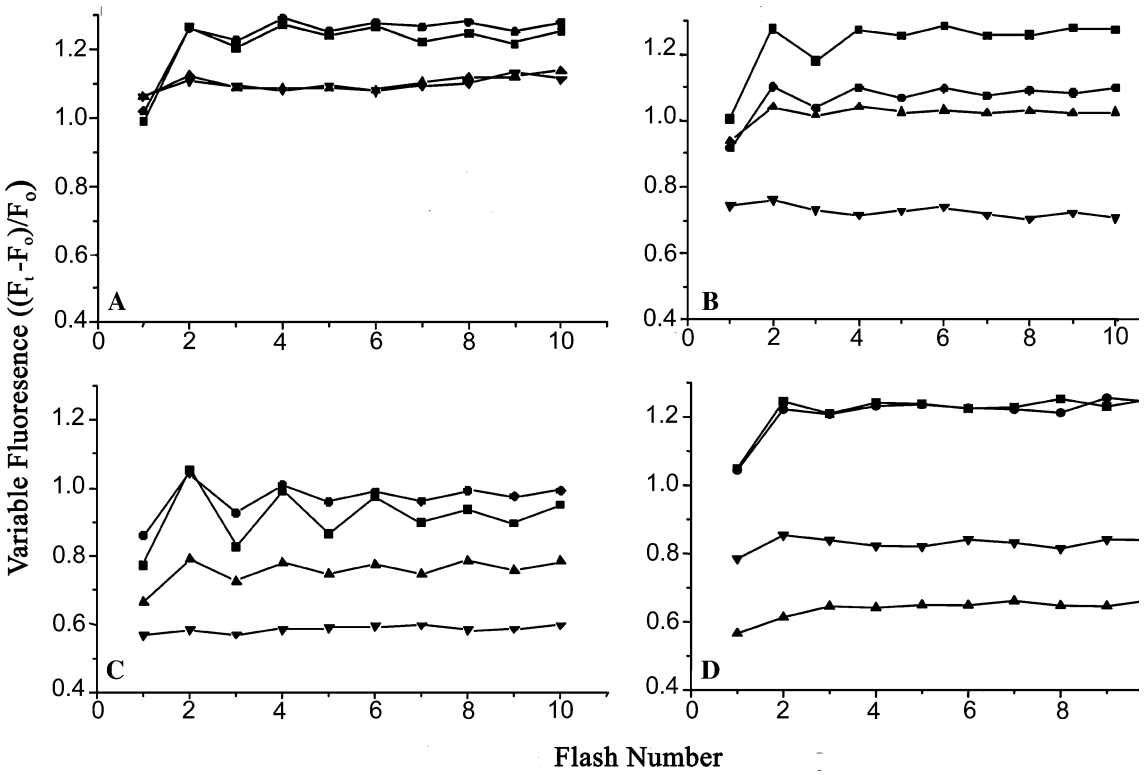

Fig. 6 Binary oscillations in Chl *a* fluorescence: the two-electron gate on the acceptor side of PS II. Panel **A** shows variable Chl *a* fluorescence data at 195 μs after a series of flashes, given at 1 Hz, for the wild type *C. reinhardtii cells*; panel **B** is for R257K; panel **C** is for R257Q; and panel **D** is for R257E mutant cells. Cells were treated with 100 μM (squares), 50 μM (circles), 25 μM (triangles), and 10 μM (inverted triangles) of *p*-benzoquinone. F_t is fluorescence at time *t*, and F_0 is the initial minimal fluorescence. [Chl], 7 μg/ml

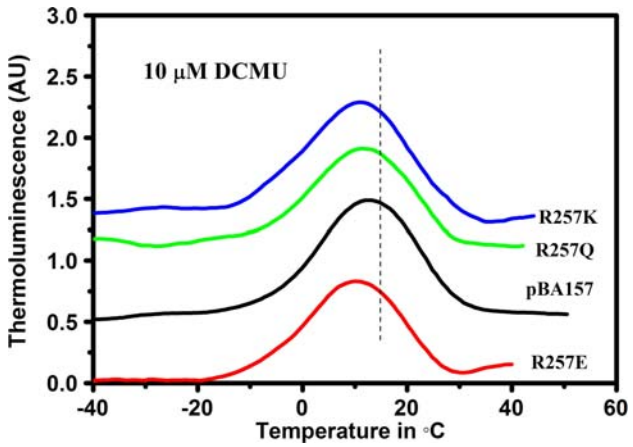

Fig. 7 Thermoluminescence curves from DCMU-treated cells. Data show the Q-band (due to $S_2Q_A^-$ recombination) in *C. reinhardtii* cells from wild type (pBA157) and three D1-R257 mutant strains (R257K, R257Q, and R257E). Note that in all cases the Q-band is at ~10°C suggesting that the mutation did not change the Q_A/Q_A^- redox potential. Thermoluminescence curves were staggered vertically for clarity. For details, see text

temperature thermoluminescence peak (or shoulder) for the untreated wild type cells in Fig. 8 (panel A) has a maximum at about 10°C. Pre-treating the cells with 25 μM BQ (Fig. 8, panel B) results in a curve which retains both bands. An increase of 2°C in the mean peak temperature was observed, but we do not regard this as significant. Pretreatment of the wild type cells with 100 μM BQ leads to a loss of most of the thermoluminescence at the smaller peak in the 10–15°C range (the Q-band). However, the 35–40°C band (the B-band) was retained (Fig. 8, panel C). The mean peak temperature of this band changes less than 1°C after the 100 μM BQ pretreatment. Further details on the mutants are as follows.

D1-R257K

For the R257K mutant, the thermoluminescence curve, when no inhibitor was present and there was no pretreatment with BQ, showed a major peak at ~32°C (B band) and a shoulder (Q band) at ~0°C (Fig. 8, panel A). However, the mean peak temperature of the B band was approximately 8°C lower than in the wild type (pBA157) cells, and the Q band was a weak shoulder. The thermoluminescence peak (B band) with 25 μM BQ was not much different (Table 4), but the weak shoulder (Q band) was much weaker. Pretreatment with 100 μM BQ resulted in a reduced overall intensity; however, the temperature of the peak did not significantly change (Fig. 8, panel C).

Table 4 Mean peak locations of thermoluminescence curves

Strain	10 μM DCMU (°C)	No addition (°C)	25 μM BQ (°C)	100 μM BQ (°C)
Control	13.16 ± 0.36	41.93 ± 0.50	43.90 ± 0.54	43.16 ± 0.06
R257E	11.25 ± 0.83	32.04 ± 0.41	31.52 ± 0.52	No signal
R257K	12.39 ± 0.70	32.15 ± 0.32	34.75 ± 0.10	33.50 ± 0.20
R257Q	13.64 ± 0.12	31.84 ± 0.06	30.20 ± 0.45	36.62 ± 0.32

D1-R257Q

The thermoluminescence data for the R257Q mutant shows two distinct peaks (Fig. 8, panel A). However, the major peak (B band) is shifted to 30°C, 10°C lower than in the wild type cells; however, a smaller peak at lower temperature (Q band) is located in the same range as that of the wild type. The two peaks seen in the curves for the untreated and 25 μM BQ-treated (Fig. 8, panels A and B) R257Q cells are much closer in size than the two peaks in the wild type cells. The mean peak temperature of thermoluminescence from the R257Q strain after pretreatment with 25 μM BQ was close to the mean peak temperature for untreated R257Q cells (1.6°C different). After pretreatment with 100 μM BQ, there remains only the higher temperature peak, but it shifts to a higher temperature by ~6°C (Fig. 8, panel C).

D1-R257E

For the R257E mutant, the thermoluminescence curve shows a peak at 30°C (B band). However, a small signals in the 0–20°C range (Q band; cf. Fig. 8, panels A with B), after pretreatment with 25 μM BQ was unexpected. The mean peak locations for the R257E mutant are close to the mean peak locations for the R257Q mutant under the same experimental conditions, while the R257K mutant has a higher peak temperature. After pretreatment with 100 μM BQ, almost all the thermoluminescence signal was lost (Fig. 8, panel C).

A comparison between the mutants

As noted above, the thermoluminescence curves, after treatment with 25 μM BQ, showed the same general results as the untreated cells except the R257E cells. When the cells were pretreated with 100 μM BQ, a markedly different behavior was observed (cf. Fig. 8, panels A with C). While R257K mutant cells gave an approximately similar curve with and without the 100 μM BQ treatment, the R257Q mutant and the wild type control showed a significant decrease of the low temperature (~10°C) Q band and single large peaks at ~37 and ~43°C (B bands), respectively, as expected if the oxidation of the plastoquinone pool was more complete at this higher concentration of BQ; these high temperature peaks had up-shifted by ~3 and 8°C from the untreated samples. The loss of essentially all thermoluminescence peak amplitudes for R257E after 100 μM BQ treatment is discussed more extensively below.

Analysis of thermoluminescence

Thermoluminescence curves were analyzed as outlined in the "Materials and Methods" section, using an extension of the Rappaport et al. (2005) treatment. Values for the apparent equilibrium constant derived from ΔG values, obtained by fitting the data, are summarized in Table 5. For untreated samples, the free-energy (ΔG) values of all the three R257 mutants are in the range of −40 mV, whereas that of the wild type is in the range of −70 mV. Further, the apparent equilibrium constant (K'_{app}) values of the three mutants were almost one-third of that of the wild type. For further information, see Table 5 and "Discussion" section.

Discussion

In this study, several mutants (R to E, Q, and K) constructed at arginine257 (R257) in D1 protein of the PS II in *C. reinhardtii* were characterized by photoautotrophic growth curve, steady-state oxygen evolution, thermoluminescence, Chl *a* fluorescence decays after two turn-over flashes, and after a single turn-over flash in the presence of DCMU. Also studied was the binary oscillation pattern of variable Chl *a* fluorescence of the R257 mutants compared to the wild type after a series of exciting actinic flashes, at a frequency of 1 Hz, that were given to samples pretreated with different concentrations of BQ.

Position of D1-R257 relative to electron transfer to the Q_B-binding pocket

The arginine at position 257 of the D1 protein of PS II is highly conserved, as is the rest of the D1 sequence forming the Q_B site. Crystallographic models show that R257 is close to the Q_B-binding domain with its side chain extending away from the pocket and into the stromal

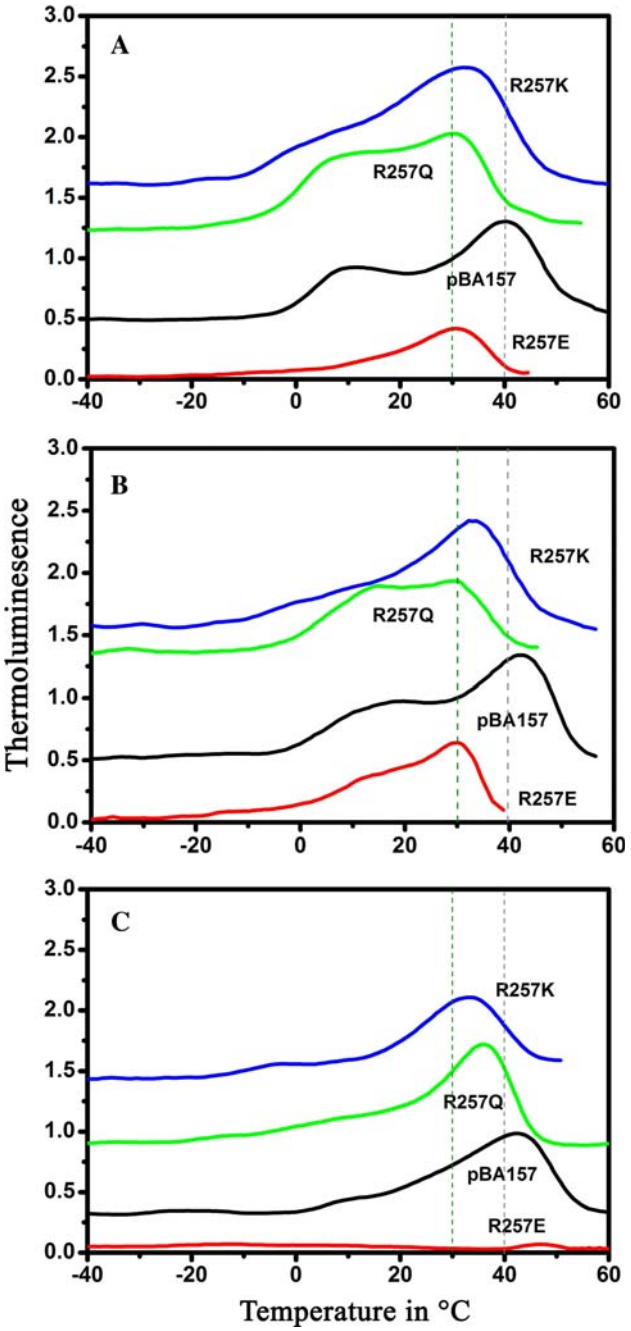

Fig. 8 Thermoluminescence curves of *C. reinhardtii* cells. Panel **A** is for the untreated cells of wild type (pBA157) and three D1-R257 mutant strains (R257K, R257Q, and R257E). Panel **B** is for 25 μM BQ, and panel **C** is for 100 μM BQ-treated cells. Thermoluminescence curves were staggered vertically for clarity. The ordinate is plotted in arbitrary units (AU)

aqueous phase as shown in Fig. 1 (coordinates from Protein Databank file 2AXT; see reviews on structure of PS II in Wydrzynski and Satoh 2005).

In the Ferreira et al. (2004) structure, the R257 side chain does not form any close interaction with neighboring groups but may interact coulombically with a highly polar span (K23–R24–D25–R26) in the D2 subunit, in which the aspartic residue (D25) is the closest side chain, at ~4.0 Å. However, these side chains are in the aqueous phase, so electrostatic effects would be somewhat damped by the shielding of the charges by the surrounding water molecules. The histidine residue (H252), located in the de-helix of D1, forms a cap over the Q_B-binding pocket; this predominantly positively charged patch is expected to exert a surface charge effect that would favor anionic and disfavor cationic groups. As a consequence, the local pH would be raised. If H^+-uptake were limiting, this would slow PS II turnover by lowering the probability of H^+ donation to the site. The group of positively charged residues might also be expected to exert an electrostatic field that would favor electron transfer to form Q_B^- in the site by a coulombic effect.

In the Loll et al. (2005) model, the local structure is somewhat different (Fig. 1). The glutamine residue (D1-Q261) is located within H-bonding distance of R257, while on the stromal side of the protein, a strand from CP47 crosses the top of the de-helix, and this strand provides an additional H-bond from the glutamate residue (E489) to R257. The negative charge from these residues would diminish the electrostatic and surface charge effects expected on the basis of the Ferreira et al. (2004) model.

Based on homology modeling with bacterial reaction centers, D1-H252 of this group of residues is a likely candidate to account for the pH dependence of the reactions of the two-electron gate (Taoka et al. 1983; Crofts et al. 1987; Petrouleas and Crofts 2005). Xiong et al. (1996, 1998b) suggested that a channel to conduct protons might exist in the PS II D1/D2 proteins, but the surface location of H252 argues against any necessity for an extended channel at the distal end of the Q_B pocket. The structural evidence (Ferreira et al. 2004; also see Kern and Renger 2007) shows that D1-R257 is ~9 Å from D1-H252. The latter is suggested to interact with the catalytic site through participation in H-bond exchange with the serine residue (S264), which in turn can also H-bond to the Q_B carbonyl oxygen (Crofts et al. 1987, 1993; Taoka 1989; Petrouleas and Crofts 2005). The D1-H252 residue is likely to facilitate H^+ exchange, and mutagenesis suggests that it is responsible for the pH dependence of the first electron transfer reaction (S. Padden and A. R. Crofts, unpublished). Protonation of D1-H252 on formation of Q_B^- would stabilize the semiquinone and increase the equilibrium constant favoring the reduction of plastoquinone by Q_A^-.

Although the structural evidence is ambiguous with respect to a functional role of the residue at position 257, the most plausible effect of mutagenesis at this position on catalysis would be through modification of electrostatic interactions, either to perturb the p*K* of D1-H252 and/or to shift the E_m of the Q_B/Q_B^- couple. Any direct participation

Table 5 Values for free energy and equilibrium constant derived from thermoluminescence curves by peak analysis

Strain	No addition			25 μM BQ			100 μM BQ		
	T_m (°C)	ΔG (mV)	K'_{app} (T_m)	T_m (°C)	ΔG (mV)	K'_{app} (T_m)	T_m (°C)	ΔG (mV)	K'_{app} (T_m)
Control	41.93	−70.3	13.33	43.9	−75.6	15.93	43.16	−73.6	14.90
R257E	32.04	−42.6	5.05	31.52	−41.06	4.78	n/a	n/a	n/a
R257K	32.15	−42.9	5.11	34.75	−50.5	6.71	33.5	−46.9	5.90
R257Q	31.84	−42.01	4.95	30.20	−37.1	4.14	36.62	−55.7	8.06

Parameters for the peak analysis giving the solutions shown were $B = 0.7$°C/s; $\Delta S_{ex} = 0.001786$; $\Delta H_{ex} = 0.685$ V; $\Delta S_r = 0.001992$; $\Delta H_r = 0.637$ V; $\Delta S_d = 0.000357$; $\Delta H_d = 0.230$ V. Values for ΔS_r, ΔS_d, and ΔH_d were taken from Rappaport et al. (2005), and the values for ΔH_r and ΔH_{ex} were calculated from peak analysis of the Q-band in the presence of DCMU. ΔG and K'_{app} are the free-energy change and equilibrium constant for the reaction $Q_A^-Q_B \leftrightarrows Q_AQ_B^-$ (where Q_B^- represents semiquinone in all states of protonation)

in catalysis or substrate selectivity seems highly unlikely. An indirect role such as that suggested here would be sufficient to provide an explanation for its conserved nature. The role in bicarbonate-reversible formate binding (see a review by Govindjee and van Rensen 1993) is more difficult to explain, since the structures show that bicarbonate (carbonate), the reactant that formate is supposed to displace, is some 20 Å away. However, the positive surface charge in the native structure might act to attract anionic residues to the locale. Loss of a charge would reduce this effect, and reversal of the charge would reduce it even further.

Thermoluminescence

As discussed in earlier sections, the thermoluminescence signal is the sum of luminescence signals generated by different populations of centers, corresponding to different product states from which the electron–hole pairs are detrapped, and this depends on the competing pathways for recombination, and the redox driving force, as determined by the state of the acceptor side. In the current thermoluminescence experiments, the stable states of PS II available for charge recombination after a single saturating flash in DCMU-treated cells should be $S_2Q_A^-$ (75%) and $S_1Q_A^-$ (25%), while in the absence of DCMU, the product states will be $S_2[Q_A^-Q_B] \leftrightarrows S_2[Q_AQ_B^-]$ (75%) and $S_1[Q_A^-Q_B] \leftrightarrows S_1[Q_AQ_B^-]$ (25%). The presence of 18-Crown-6 minimized any possible effect due to the proton gradient, so changes in thermoluminescence are mainly due to changes in redox free energy and are largely determined by the state of the acceptor side and by the equilibrium constant favoring the Q_B^- state.

The peak temperature of a thermoluminescence component is indicative of the energy stored in the charge separated pair, determined by redox state of both the recombination partners. The results show that the three mutant and the wild type cells all had a Q-band with peak temperature in the same range (Fig. 7). This demonstrates that the overall stability of $S_2Q_A^-$ charge pair was not affected by the mutations at R257. Thus, assuming that DCMU has no differential effect in the mutant strains, and that effects of mutation were restricted to the acceptor side, we suggest that the redox potential of Q_A/Q_A^- pair is unaffected by the mutations at D1-R257.

The small peak of the thermoluminescence curve, observed at the same position as the Q-band, is most likely due to the $S_2Q_A^-$ charge recombination and may also include a contribution from "non-Q_B centers" (see below). Since all the mutants we examined show a normal Q-band when the electron sharing between Q_A and Q_B was blocked by DCMU, the large peaks at around 30°C must be due to $S_2Q_B^-$ charge recombination, each representing a modified B-band. The shift of these peaks to lower temperature in the mutants would therefore indicate that the stability of $S_2Q_B^-$ charge pair was lowered in these mutants, indicating that the equilibrium constant favoring Q_B^- was lowered, and hence the effective E_m of the quinone Q_B/semiquinone Q_B^- couple was lowered.

The variability in size of the Q- and B-band peaks observed in the thermoluminescence curves of untreated cells calls for further discussion, since the amplitude of the Q-band peak is larger than normally observed in thylakoids. This could be attributed to a scrambling of the two-electron gate associated with a higher degree of reduction of the plastoquinone pool, but the BQ treatment was designed to minimize this. Any effect would have to be attributed to re-equilibration with endogenous metabolism after the washing of BQ. An additional possibility is an unusual preponderance of non-functional, the so-called "non-Q_B-reducing," centers (Lavergne and Leci 1993; Lavergne and Briantais 1996). Although the ratio of Q_B-reducing to non-Q_B-reducing centers is not known in our *C. reinhardtii* samples, the slowly decaying phase of the Q_A^- oxidation is variable between the samples used, and with different growth conditions, and such variability was also observed in the mutant cells. If we assume that the variability in amplitude of the lower (Q-band) peak was largely due to a combination of these effects, then we can simplify the interpretation of the data by concentrating on the B-band changes. We show that the three mutants (E, K,

and Q) at R257 all have downshifted B-bands, which originate mainly from the $S_2Q_B^-$ charge recombination, and this is most obvious after BQ treatment. Therefore, we conclude that these mutants are specifically affected in the recombination of the $S_2Q_B^-$ charge pair. Although a shift in thermoluminescence peak temperature could possibly result from an influence on the donor-side, the fact that the Q-band is unmodified argues strongly against that possibility. In contrast, the effects on the B-band clearly indicate that the mutations affect the acceptor side, and the constancy of the Q-band suggests that they are localized to the Q_B site (Table 2).

The rate constants

In our previous study (Xiong et al. 1998a), we measured flash-induced fluorescence yield decay kinetics in the D1-R257M and D1-R257E mutants and had analyzed these in terms of the model proposed by Crofts and coworkers (see review by Petrouleas and Crofts 2005). In this analysis, the decay kinetics were deconvoluted into three components, with characteristic times, or lifetimes, in the range 150–200 μs, 2 ms, and >100 ms. The first two components reflect, respectively, the electron transfer in centers which have a bound plastoquinone at the time of the flash and centers in which electron transfer awaits binding of plastoquinone from the membrane. The long-lived decay reflects in part the fraction of $Q_A^-Q_B$ remaining in equilibrium with $Q_AQ_B^-$, and in part non-functional (non-B) centers, with the relative contributions varying for a variety of conditions. In these two mutants, the ~200 μs phase reflecting electron flow, $Q_A^-Q_B$ to $Q_AQ_B^-$, determined by rate constant k_{AB}, did not significantly differ from the wild type control.

The apparent equilibrium constant, K_{app}, determining the fraction of centers with an electron on Q_B, is determined by contributions from the equilibrium constant for electron transfer, K_E, the pK of the group stabilizing Q_B^- (pK_3 determining, e.g., the protonation of D1-H252), and the binding constant for plastoquinone at the site, K_O, as shown in Eq. 12 and Scheme 1. At constant pH, these three terms can be treated as a single term. K_{app}, the measured equilibrium constant, is then given by

$$K_{app} = \frac{K_E}{1 + K_O} \frac{\left(1 + \frac{[H^+]}{K_3}\right)}{\left(1 + \frac{[H^+]}{K_1}\right)} \quad (12)$$

The shifted thermoluminescence peaks point to an explanation in terms of a lowered value for K'_{app} (see Petrouleas and Crofts 2005), but because the forward rate constants were unaffected, this would have to come from a higher rate for the reverse electron transfer between $Q_AQ_B^-$ and $Q_A^-Q_B$. A larger relative amplitude of the slower kinetic component compared to the wild type was observed

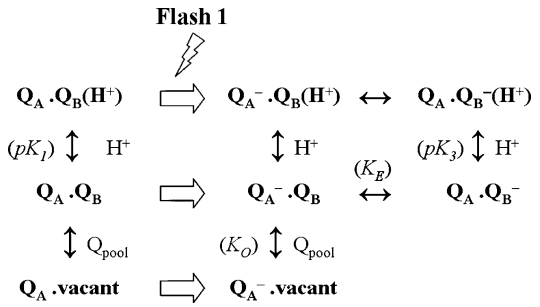

Scheme 1 The equilibria in the acceptor complex determining K_{app}

in both the R257M and R257E mutants, which could be ascribed to a lower value for the equilibrium constant for electron transfer, K_E, or weaker binding of plastoquinone. As mentioned earlier, we have incorporated the Crofts et al. (1993) model of the equilibria of the two-electron gate into the Rappaport kinetic model for thermoluminescence (Rappaport et al. 2005), using a free-energy approach (De Vault and Govindjee 1990) to represent the trapped states. Implementation of the model generated simulated thermoluminescence curves that matched the measured data, confirming the validity of this approach. In this context, the results seem to be well explained by an electrostatic effect on K'_{app} (Table 5).

The values of the three equilibrium constants making up K'_{app} in the wild type pertain to the native electrostatic field, and the mutations would modify the field by making it less positive. Since plastoquinone is a neutral species, no electrostatic effect would be anticipated on K_O, unless through its pH dependence. Nevertheless, the increased relative amplitude of the slow phase in the fluorescence yield decay would be compatible with a weaker affinity for plastoquinone, which could reflect effects on pK_1 and pK_2 contributing to K_O. The native field would favor electron transfer to form Q_B^-, and any lessening of the field would thus change K_E to favor a distribution more in favor of Q_A^-. Changes in the electrostatic effects leading to pK_3 (and hence affecting the apparent equilibrium constant) would represent an interplay between the field from Q_B^- and that from the surface residues, which would change on mutation of D1-R257. Detailed modeling of electrostatics of the site would be required to pin down specific effects, and discrimination between effects on K_E, K_O, and pK_3 must await experimental evidence from detailed studies of pH dependence of the two-electron gate equilibria in the mutant and wild type strains.

Anomalous effects of benzoquinone

Treatment of *C. reinhardtii* with BQ has several effects. As mentioned earlier, our purpose in adding BQ was to oxidize the plastoquinone pool, and hence the occupant of the Q_B site, so as to set a consistent initial starting state. Other effects

of BQ addition are inhibition of metabolism, collapsing of the transmembrane electrical potential, and at high concentrations, occupancy of the Q_B site by BQ redox intermediates that result in anomalous kinetics (Lavergne 1982; Taoka et al. 1983). Although the BQ treatment by Cuni et al. (2004) increased the lifetime of the $S_2Q_A^-$ state at 20°C in a manner consistent with the effect of collapsing the membrane potential, our inclusion of 18-Crown-6 would mean that no membrane potential should develop, so this effect of BQ can be ignored. The addition of BQ in fluorescence experiments can also cause quenching of the fluorescence intensity, which would change the fluorescence yield by introduction of an additional quenching pathway. In our treatment of the cells after incubation with BQ, the cells were washed, centrifuged, and resuspended in buffer without any BQ. Although the BQ results are not fully understood, several aspects provide additional information that point to interesting differences between mutant strains.

One interesting result was the unexpected behavior of the B-band from cells treated with higher concentration of BQ (Fig. 8). In intact systems, the ratio of Q_B and Q_B^- is 50:50 (Rutherford et al. 1984). The BQ treatment was expected to oxidize both the pool plastoquinones and the bound species in equilibrium with the pool and to minimize the effects of other metabolic interactions, allowing for a more homogeneous state of Q_B (Lavergne and Leci 1993). In dark-adapted spinach chloroplasts, a ratio of 70% Q_B and 30% of Q_B^- was reported (Wollman 1978; also see Shinkarev and Wraight 1993), but Robinson and Crofts (1983) showed that treatment of thylakoids with low concentration of BQ led to complete oxidation of the Q_B occupant. We expected that with the BQ treatment, the Q_B site would be occupied by a quinone so that a single peak would be expected at the B-band position in thermoluminescence curves. Since we used whole cells, additional complications might be expected. The effects of BQ were found to be very concentration dependent. Low concentrations had little effect, but at 100 μM or higher, the expected increase in the B-band was observed for wild type controls (where the B-band was at about 40°C), and in the R257K and R257Q mutants (where it was around 30°C). The thermoluminescence curves showed peaks predominantly at the B-band position, and the loss of amplitude at the Q-band could be explained by equilibration of the two-electron gate components with the more oxidized quinone pool. The most dramatic effect of the 100 μM BQ treatment was in the R257E mutant. The loss of any significant thermoluminescence signal could have several explanations. Since no Q-band was seen in the absence of DCMU, the loss of the B-band could not be explained simply by a modification of the Q_B site so as to inhibit the electron transfer between Q_A and Q_B. A plausible alternative is that plastoquinone was replaced by BQ, which provided a more stable acceptor. We note that BQ at high concentrations has been shown to displace the endogenous plastoquinone from the Q_B site in thylakoids and to accept an electron to generate the semiquinone state (Lavergne 1982; Taoka et al. 1983). However, the DCMU titer was not changed in the mutant strains, showing that no gross modification of the site affecting DCMU binding occurred. None of the mutants showed a large difference between the fluorescence yield at the first point of measurement (at 65 μs) in the presence or absence of DCMU (Figs. 3–5), suggesting a quenching independent of occupancy. Another possibility is that the structure was sufficiently destabilized (see below) as to allow easier access of BQ to Chl from the antenna, allowing quenching and a loss of fluorescence yield, as seen directly in the fluorescence data (Figs. 3–5). The fluorescence yield also determines the thermoluminescence yield (Eqs. 8, 9); thus, the loss of fluorescence intensity would be reflected in an equivalent loss in thermoluminescence. However, in the present experiments, care was taken to wash excess BQ from the preparation before the experiments, so a residual effect would be unlikely unless mutation had given rise to a tight binding of BQ or its semiquinone.

Pleiotropic effects resulting from changes in structural stability

An additional point needs to be stressed in the analysis of our results. In the discussion of the environment of R257 above, a location close to an interface between the D1 subunit and both the D2 and CP47 subunits was mentioned. The distances between R257 of D1 and D25 of D2 (2.8 or 4 Å, depending on the model), or E489 of CP47, would result in either a H-bond or a coulombic (electrostatic) attraction that would contribute to the stability of the protein. Any change in the electric charge on substitution of R257 (as in the mutations here) would change these interactions, with a differential effect on the stabilizing force. The fact that all mutants were functional suggests that no large-scale pleiotropic effects resulted, but we cannot exclude smaller effects that might have led to a departure from the null condition assumed in our analysis. In particular, the differential effects of BQ treatment on fluorescence yield in the mutant strains might reflect the introduction of a 'looser' structure that would allow a quenching interaction between BQ and antenna pigments. However, any more detailed analysis would require structural data that are not yet available.

Stability of Q_A/Q_A^- and Q_B/Q_B^- in other systems

Mäenpää et al. (1995) showed that mutation in the D–E loop of the D1 protein (D1-E243K, E229D, Q241H, among others), of *Synechocystis* sp PCC 6803, had shifted "Q" and "B" thermoluminescence bands, and, thus, the stability of both the Q_A/Q_A^- and Q_B/Q_B^- couples was suggested to be

affected. Mulo et al. (1997) showed that the Q_B site was severely perturbed in the deletion mutants (ΔR225–F239, ΔG240–V249, and ΔR225–V249), also from *Synechocystis* sp. PCC 6803. Since no theoretical analysis was made in these studies, no quantitative data are available on the redox potential changes. On the other hand, Keranen et al. (1998) observed that there was no difference in the peaks of the "Q" and "B" thermoluminescence bands between autotrophic and heterotrophic cells of *Synechocystis* sp. PCC 6803. Further research is needed to obtain a clear picture of the relationship between the shifts in the "Q" and the "B" thermoluminescence bands, the binding niches of Q_A/Q_A^- and Q_B/Q_B^- and their redox potentials not only in *Synechocystis* sp. PCC 6803, but also in *C. reinhardtii*.

Conclusions

We conclude that, although the forward rate of electron transfer between Q_A and Q_B is little affected, the two-electron gate on the acceptor side PS II is thermodynamically perturbed in the R257 mutants. The perturbation in the electron transfer between the primary and secondary plastoquinone led to a decrease in the overall electron transfer rate from water to plastoquinone, which further led to the decreased saturation level in the photoautotrophic growth. The effects on equilibrium constants of the two-electron gate are likely due to changes in coulombic fields on changing the net charge in the neighborhood of the Q_B site, suggesting that the electrostatic environment plays an important role in mechanism. The bicarbonate-reversible formate effect on the Q_B site has been shown to be on the protonation events at this site (Eaton-Rye and Govindjee 1988a, b). Dramatic differences of the bicarbonate effect on the D1-R257 mutants, observed earlier (Xiong et al. 1998a), thus might have a basis on the changes in the redox potential and the stability of the Q_B site, observed in this paper.

Acknowledgments Govindjee acknowledges support from the Department of Plant Biology, University of Illinois at Urbana-Champaign; ARC and SWR acknowledge support from NIH GM35438; JM acknowledges support from MEXT 18GS0318. MS acknowledges support from the Cooperative State Research, Education and Extension Service, U.S. Department of Agriculture, Project No. ILLU-875-389. We thank Jan Kern for discussions on the location of bicarbonate ions on the Photosystem II reaction center. We also thank George Papageorgiou for reading the final draft of this manuscript and for making valuable suggestions to improve the readability of this article.

References

Amesz J, Fork DC (1967) Quenching of chlorophyll fluorescence by quinones in algae and chloroplasts. Biochim Biophys Acta 143:97–107. doi:10.1016/0005-2728(67)90114-4

Blubaugh DJ, Govindjee (1988) The molecular mechanism of the bicarbonate effect at the plastoquinone reductase site of photosynthesis. Photosynth Res 19:85–128. doi:10.1007/BF00114571

Bowes JM, Crofts AR (1980) Binary oscillations in the rate of reoxidation of the primary acceptor of Photosystem-II. Biochim Biophys Acta 590:373–384. doi:10.1016/0005-2728(80)90208-X

Bowes JM, Crofts AR (1981) Effect of DBMIB on the secondary electron acceptor B of Photosystem II. Arch Biochem Biophys 209:682–686. doi:10.1016/0003-9861(81)90329-5

Bowyer J, Hilton M, Whitelegge J, Jewess P, Camilleri P, Crofts A et al (1990) Molecular modeling studies on the binding of phenylurea inhibitors to the D1 protein of Photosystem II. Z Naturforsch 45c:379–387

Bouges-Bocquet B (1973) Electron transfer between two photosystems in spinach chloroplasts. Biochim Biophys Acta 314:250–256. doi:10.1016/0005-2728(73)90140-0

Crofts AR, Wraight CA, Fleischman DE (1971) Energy conservation in the photochemical reactions of photosynthesis and its relation to delayed fluorescence. FEBS Lett 15:89–100. doi:10.1016/0014-5793(71)80031-5

Crofts AR, Robinson HH, Andrews K, Van Doren S, Berry E (1987) Catalytic sites for reduction and oxidation of quinones. In: Papa S, Chance B, Ernster L (eds) Cytochrome systems: molecular biology and bioenergetics. Plenum Publ, New York, pp 617–624

Crofts AR, Baroli I, Kramer D, Taoka S (1993) Kinetics of electron transfer between Q_A and Q_B in wild-type and herbicide-resistant mutants of *C. reinhardtii*. Z Naturforsch 48c:259–266

Cuni A, Xiong L, Sayre R, Rappaport F, Lavergne J (2004) Modification of the pheophytin midpoint potential in Photosystem II: modulation of the quantum yield of charge separation and of charge recombination pathways. Phys Chem Chem Phys 6:4825–4831. doi:10.1039/b407511k

De Vault D, Govindjee (1990) Photosynthetic glow peaks and their relationship with the free-energy changes. Photosynth Res 24:175–181

De Vault D, Govindjee, Arnold W (1983) Energetics of photosynthetic glow peaks. Proc Natl Acad Sci USA 80:983–987. doi:10.1073/pnas.80.4.983

Ducruet J-M, Peeva V, Havaux M (2007) Chlorophyll thermofluorescence and thermoluminescence as complementary tools for the study of stress in plants. Photosynth Res 93:159–171. doi:10.1007/s11120-007-9132-x

Eaton-Rye JJ, Govindjee (1988a) Electron transfer through the quinone acceptor complex of Photosystem II in bicarbonate-depleted spinach thylakoid membranes as a function of actinic flash number and frequency. Biochim Biophys Acta 935:237–247. doi:10.1016/0005-2728(88)90220-4

Eaton-Rye JJ, Govindjee (1988b) Electron transfer through the quinone acceptor complex of Photosystem II after one or two actinic flashes in bicarbonate-depleted spinach thylakoid membranes. Biochim Biophys Acta 935:248–257. doi:10.1016/0005-2728(88)90221-6

Ferreira KN, Iverson TM, Maghlaoui K, Barber J, Iwata S (2004) Architecture of the photosynthetic oxygen-evolving center. Science 303:1831–1838. doi:10.1126/science.1093087

Gorman DS, Levine RP (1965) Cytochrome *f* and plastocyanin: their sequence in the photosynthetic electron transport chain of *Chlamydomonas reinhardtii*. Proc Natl Acad Sci USA 54:1665–1669. doi:10.1073/pnas.54.6.1665

Govindjee, Van Rensen JJS (1993) Photosystem II reaction centers and bicarbonate. In: Deisenhofer J, Norris JR (eds) Photosynthetic reaction centers, vol 1. Academic, Orlando, pp 357–389

Govindjee, Pulles MPJ, Govindjee R, van Gorkom HJ, Duysens LNM (1976) Inhibition of the reoxidation of the secondary electron acceptor of Photosystem II by bicarbonate depletion. Biochim Biophys Acta 449:602–605

Harris EH (1988) The *Chlamydomonas* sourcebook: a comprehensive guide to biology and laboratory use. Academic, San Diego

Humphrey W, Dalke A, Schulten K (1996) VMD—visual molecular dynamics. J Mol Graph 14:33–38. doi:10.1016/0263-7855(96)00018-5

Inoue Y (1996) Photosynthetic thermoluminescence as a simple probe of Photosystem II electron transport. In: Amesz J, Hoff AJ (eds) Biophysical techniques in photosynthesis, advances in photosynthesis and respiration, vol 3 (series editor: Govindjee). Kluwer Academic Publishers (now Springer), Dordrecht, pp 93–107

Kern J, Renger G (2007) Photosystem II: structure and mechanism of water:plastoquinone oxidoreductase. Photosynth Res 94:183–202. doi:10.1007/s11120-007-9201-1

Keranen M, Pulo P, E-M Aro, Govindjee, Tyystjärvi E (1998) Thermoluminescence B and Q bands are the same temperature in an autotrophic and a heterotrophic D1 protein mutant of *Synechocystis* sp. PCC 6803. In: Garab G (ed) Photosynthesis mechanisms and effects. Kluwer Academic Publishers (now Springer), Dordrecht, pp 1145–1148

Kok B, Forbush B, McGloin M (1970) Cooperation of charges in photosynthetic O_2 evolution—I. A linear four step mechanism. Photochem Photobiol 11:457–475. doi:10.1111/j.1751-1097.1970.tb06017.x

Kramer DM, Crofts AR (1990) A portable multi-flash fluorimeter for measurement of donor and acceptor reactions of Photosystem 2 in leaves of intact plants under field conditions. Photosynth Res 26:181–193. doi:10.1007/BF00033131

Kramer D, Adawi O, Morse PII, Crofts AR (1987) A portable double-flash spectrophotometer for measuring the kinetics of electron transport components in intact leaves. In: Biggins J (ed) Progress in photosynthesis research, vol 2. Martinus Nijhoff Publishers, Dordrecht, pp 665–668

Kramer DM, Roffey RA, Sayre RT, Govindjee (1994) The A(T) thermoluminescence band from *Chlamydomonas reinhardtii* and the effects of mutagenesis of histidine-residues on the donor side of the Photosystem II D1 polypeptide. Biochim Biophys Acta 1185:228–237. doi:10.1016/0005-2728(94)90214-3

Lavergne J (1982) Interaction of exogenous benzoquinone with Photosystem II in chloroplasts: the semiquinone form acts as a dichlorophenyldimethylurea-insensitive secondary acceptor. Biochim Biophys Acta 679:12–18. doi:10.1016/0005-2728(82)90249-3

Lavergne J (1984) Absorption changes of Photosystem II donors and acceptors in algal cells. FEBS Lett 173:9–14. doi:10.1016/0014-5793(84)81006-6

Lavergne J, Briantais JM (1996) Photosystem II heterogeneity. In: Ort DR, Yocum C (eds) Oxygenic photosynthesis: the light reactions. Advances in photosynthesis and respiration (series editor: Govindjee), vol 4. Kluwer Academic Publishers (now Springer), Dordrecht, pp 265–287

Lavergne J, Leci E (1993) Properties of inactive Photosystem II centers. Photosynth Res 35:323–343. doi:10.1007/BF00016563

Lavorel J (1968) Sur une relation entre fluorescence et luminescence dans les systemes photosynthetique. Biochim Biophys Acta 153:727–730. doi:10.1016/0005-2728(68)90203-X

Loll B, Kern J, Saenger W, Zouni A, Biesadka J (2005) Towards complete cofactor arrangement in the 3 0 Å resolution structure of Photosystem II. Nature 438:1040–1044. doi:10.1038/nature04224

Mäenpää P, Miranda T, Tyystjärvi E, Govindjee, Tyystjärvi T, Ducruet J-M, Etienne A-L, Kirilovsky D (1995) A mutation in the D-de loop of D1 modifies the stability of the $S_2Q_A^-$ and $S_2Q_B^-$ states in Photosystem II. Plant Physiol 107:187–197

Minagawa J, Crofts AR (1994) A robust protocol for site-directed mutagenesis of the D1 protein of *Chlamydomonas reinhardtii*: a PCR-spliced *psbA* gene in a plasmid conferring spectinomycin resistance was introduced into a *psbA* deletion strain. Photosynth Res 42:121–131. doi:10.1007/BF02187123

Moser CC, Page CC, Chen X, Dutton PL (1997) Biological electron tunneling through native protein media. J Biol Inorg Chem 2:393–398. doi:10.1007/s007750050149

Moser CC, Page CC, Dutton PL (2006) Darwin at the molecular scale: selection and variance in electron tunneling proteins including cytochrome c oxidase. Philos Trans R Soc 361:1295–1305. doi:10.1098/rstb.2006.1868

Mulo P, Tyystjärvi T, Tyystjärvi E, Govindjee, Mäenpää P, Aro E-M (1997) Mutagenesis of the D-E Loop of Photosystem II reaction centre protein D1: function and assembly of Photosystem II. Plant Mol Biol 33:1059–1071. doi:10.1023/A:1005765305956

Papageorgiou G, Govindjee (eds) (2004) Chlorophyll *a* fluorescence: a signature of photosynthesis. Advances in photosynthesis and respiration (series editor: Govindjee), vol 19. Springer, Dordrecht

Petrouleas V, Crofts AR (2005) The iron-quinone acceptor complex. In: Wydrzynski T, Satoh K (eds) Photosystem II: the light-driven water:plastoquinone oxidoreductase. Advances in photosynthesis and respiration (series editor: Govindjee), vol 22. Springer, Dordrecht, pp 177–206

Porra RJ, Thompson WA, Kriedemann PE (1989) Determination of accurate extinction coefficients and simultaneous-equations for assaying chlorophyll-a and chlorophyll-b extracted with 4 different solvents—verification of the concentration of chlorophyll standards by atomic-absorption spectroscopy. Biochim Biophys Acta 975:384–394. doi:10.1016/S0005-2728(89)80347-0

Randall JT, Wilkins MHF (1945) Phosphorescence and electron traps I. The study of trap distributions. Proc R Soc A 184:365–389. doi:10.1098/rspa.1945.0024

Rappaport F, Guergova-Kuras M, Nixon PJ, Diner BA, Lavergne J (2002) Kinetics and pathways of charge recombination in Photosystem II. Biochemistry 41:8518–8527. doi:10.1021/bi025725p

Rappaport F, Cuni A, Xiong L, Sayre R, Lavergne RM (2005) Charge recombination and thermoluminescence in Photosystem II. Biophys J 88:1948–1958. doi:10.1529/biophysj.104.050237

Robinson HH, Crofts AR (1983) Kinetics of the oxidation reduction reactions of the Photosystem II quinone acceptor complex, and the pathway for deactivation. FEBS Lett 153:221–226. doi:10.1016/0014-5793(83)80152-5

Ruffle SV, Donnelly D, Blundell TL, Nugent JHA (1992) A 3-dimensional model of the Photosystem II reaction center of *Pisum sativum*. Photosynth Res 34:287–300. doi:10.1007/BF00033446

Rutherford AW, Crofts AR, Inoue Y (1982) Thermoluminescence as a probe of Photosystem II photochemistry—the origin of the flash-induced glow peaks. Biochim Biophys Acta 682:457–465. doi:10.1016/0005-2728(82)90061-5

Rutherford W, Govindjee, Inoue Y (1984) Charge accumulation and photochemistry in leaves studied by thermoluminescence and delayed light emission. Proc Natl Acad Sci USA 81:1107–1111. doi:10.1073/pnas.81.4.1107

Sane PV, Rutherford AW (1986) Thermoluminescence from photosynthetic membranes. In: Govindjee, Amesz J, Fork DC (eds) Light emission by plants and bacteria. Academic, Orlando, pp 329–360

Sarkar G, Sommer SS (1990) The megaprimer method of site-directed mutagenesis. Biotechniques 8:404–407

Shinkarev VP, Wraight CA (1993) Oxygen evolution in photosynthesis—from unicycle to bicycle. Proc Natl Acad Sci USA 90:1834–1838. doi:10.1073/pnas.90.5.1834

Sueoka N (1960) Mitotic replication of deoxyribonucleic acid in *Chlamydomonas reinhardtii*. Proc Natl Acad Sci USA 46:83–91. doi:10.1073/pnas.46.1.83

Taoka S (1989) Kinetics of electron transfer and binding of inhibitors in the two electron gate of chloroplasts. Ph.D. thesis, University of Illinois, Urbana-Champaign

Taoka S, Crofts AR (1987) Competition of Inhibitors with the secondary quinone in dark-adapted thylakoid membranes. In: Biggins J (ed) Progress in photosynthesis research, vol 2. Martinus Nijhoff Publishers, Dordrecht, pp 425–428

Taoka S, Robinson HH, Crofts AR (1983) Kinetics of the reactions of the two-electron gate of photosystem: studies of the competition between plastoquinone and inhibitors. In: Inoue Y, Crofts AR, Govindjee, Murata N, Renger G, Satoh K (eds) The oxygen evolving system of photosynthesis. Academic, Tokyo, pp 369–382

Van Rensen JJS (2005) Role of bicarbonate at the acceptor side of Photosystem II. In: Govindjee, Beatty JH, Gest H, Allen JF (eds) Discoveries in photosynthesis. Advances in photosynthesis and respiration (series editor: Govindjee), vol 20. Springer, Dordrecht, pp 303–310

Van Rensen JJS, Xu C, Govindjee (1999) Role of bicarbonate in the Photosystem II, the water-plastoquinone oxido-reductase of plant photosynthesis. Physiol Plant 105:585–592. doi:10.1034/j.1399-3054.1999.105326.x

Vass I (2003) The history of photosynthetic thermoluminescence. Photosynth Res 76:303–318. doi:10.1023/A:1024989519054

Vass I, Govindjee (1996) Thermoluminescence from the photosynthetic apparatus. Photosynth Res 48:117–126. doi:10.1007/BF00041002

Vassiliev S, Bruce D (2008) Toward understanding molecular mechanisms of light harvesting and charge separation in Photosystem II. Photosynth Res: 15 pp. doi:10.007/s11120-008-9203-4

Velthuys BR (1981) Electron-dependent competition between plastoquinone and inhibitors for binding to Photosystem II. FEBS Lett 126:277–281. doi:10.1016/0014-5793(81)80260-8

Velthuys BR, Amesz J (1974) Charges accumulation at the reducing side of system 2 of photosynthesis. Biochim Biophys Acta 333:85–94. doi:10.1016/0005-2728(74)90165-0

Vernotte C, Briantais J-M, Astier C, Govindjee (1995) Differential effects of formate in single and double mutants of D1 in *Synechocystis* species PCC 6714. Biochim Biophys Acta 1229:296–301. doi:10.1016/0005-2728(95)00018-E

Wollman F-A (1978) Determination and modification of the redox state of the secondary acceptor of Photosystem II in the dark. Biochim Biophys Acta 503:263–273. doi:10.1016/0005-2728(78)90187-1

Wraight CA (1981) Oxidation-reduction physical chemistry of the acceptor quinone complex in bacterial photosynthetic reaction centers: evidence for a new model of herbicide activity. Isr J Chem 21:348–354

Wydrzynski TJ, Satoh K (eds) (2005) Photosystem II: the light-driven water:plastoquinone oxidoreductase. Advances in photosynthesis and respiration (series editor: Govindjee), vol 22. Springer, Dordrecht

Xiong J, Subramaniam S, Govindjee (1996) Modeling of the D1/D2 proteins and cofactors of the Photosystem II reaction center: implications for herbicide and bicarbonate binding. Protein Sci 5:2054–2073

Xiong J, Minagawa J, Crofts A, Govindjee (1998a) Loss of inhibition by formate in newly constructed Photosystem II D1 mutants, D1-R257E and D1-R257M, of *Chlamydomonas reinhardtii*. Biochim Biophys Acta 1365:473–491. doi:10.1016/S0005-2728(98)00101-7

Xiong J, Subramaniam S, Govindjee (1998b) A knowledge-based three dimensional model of the Photosystem II reaction center of *Chlamydomonas reinhardtii*. Photosynth Res 56:229–254. doi:10.1023/A:1006061918025